Walport, F., Kucukler, M., and Gardner, L. (2022). Stability design of stainless steel structures. *Journal of Structural Engineering ASCE*, 148(1); 04021225.
https://doi.org/10.1061/(ASCE)ST.1943-541X.0003165

Stability design of stainless steel structures

F. Walport[1], M. Kucukler[2] and L. Gardner[3]

[1]Research Associate, Dept. of Civil and Environmental Engineering, Imperial College London, London, U.K. (corresponding author). E-mail: fiona.walport12@imperial.ac.uk

[2]Assistant Professor, School of Engineering, University of Warwick, Coventry, U.K. E-mail: merih.kucukler@warwick.ac.uk

[3]Professor of Structural Engineering, Dept. of Civil and Environmental Engineering, Imperial College London, London, U.K. E-mail: leroy.gardner@imperial.ac.uk

ABSTRACT

The direct analysis method (DAM), featuring second order elastic analysis with two stiffness reduction factors - τ_b and τ_g, is the primary means of stability design for steel structures in AISC 360 and AISI S100. The equivalent provisions for stainless steel structures, which are due to be incorporated into the upcoming AISC 370 and ASCE-8 Specifications are developed herein. Stainless steel exhibits a rounded stress-strain response, typically described by the Ramberg-Osgood formulation. The slope of this function (i.e. the tangent modulus), adjusted to consider the influence of residual stresses, is used to define the stiffness reduction factor τ_b at a given axial load level to be applied to members in compression to allow for the adverse influence of the spread of plasticity and residual stresses. The dependency of the degree of stiffness reduction on the roundedness of the stress-strain curve, which varies between the different grades of stainless steel is also directly captured through the strain hardening exponent n that features in the Ramberg–Osgood formulation. Values of 0.7 for AISC 370 and 0.9 for ASCE-8 are proposed for the general stiffness reduction factor τ_g to be applied to all member stiffnesses to account for the development and spread of plasticity, and to ensure a suitable reduction in stiffness for slender members with low axial load levels. The different τ_g values between the two specifications is required to reflect the different buckling curves and axial-bending interaction expressions employed. The accuracy of the proposed method for the design of stainless steel members and frames is assessed through comparisons with benchmark shell finite element results. Comparisons are also made against the new provisions in AISC 370 for design by second order inelastic analysis. The reliability of the design proposals is demonstrated through statistical analyses, where it is shown that a resistance factor ϕ of 0.9 can be adopted.

Keywords: AISC 370; Inelastic buckling; Stability; Stainless steel; Stiffness reduction; Structural design.

INTRODUCTION

The direct analysis method (DAM) in AISC 360 (AISC, 2016b) and AISI S100 (AISI, 2016) uses second order analysis to determine the internal forces in structures in the deformed configuration. The influence of material nonlinearity and residual stresses can be accounted for by either (1) performing an elastic analysis but with reduced stiffness in the members or (2) performing an inelastic analysis. In the former case, the relative simplicity of elastic analysis is retained, while in the latter case, more accurate results are achieved. The capacity of members is verified by either (1) buckling checks or (2), if initial bow imperfections are included in the members of the analysed structure, cross-section checks. In either case, the need for the determination of effective buckling lengths is eliminated (Deierlein, 2003; Kucukler, Gardner & Macorini, 2014; Surovek-Maleck & White, 2004a; Chan, Liu & Liu, 2011). Frame out-of-plumbness is accounted for in the analysis through direct modelling or through the application of notional loads. For design by second order elastic analysis, also referred to as geometrically nonlinear analysis (GNA), two stiffness reduction factors are defined: (1) a general stiffness reduction factor with a value of 0.8, referred to herein as τ_g, to be applied to all member stiffnesses to account for the development and spread of plasticity and (2) τ_b, to account for the additional reduction in flexural stiffness due to the effects of yielding and residual stresses of heavily loaded compression members. The value of $\tau_g = 0.8$ also ensures that the strength of slender members is similar to that obtained from column buckling curves (Deierlein, 2003). Further studies have been carried out to derive a single stiffness reduction factor τ_{MN} that considers fully the detrimental influence of spread of plasticity, residual stresses and member out-of-straightness on structural behavior for both steel (Kucukler, Gardner & Macorini, 2014, 2016, 2015; Kucukler & Gardner, 2018, 2019) and stainless steel (Shen & Chacón, 2020b, 2020a).

Design by elastic analysis with stiffness reduction has been developed and widely used for carbon steel structures (Surovek-Maleck & White, 2004a, 2004b; Deierlein, 2003). However, no equivalent design rules are available for application to stainless steel structures, where the influence of material yielding is more significant (Walport *et al.*, 2019). The new AISC 370 Specification (AISC, 2021) will encompass the design, fabrication and erection of hot-rolled and welded austenitic and duplex stainless steel structures. The provisions closely mirror AISC 360 (AISC, 2016b), but deviate where necessary

to account for the differences in material behavior between stainless steel and carbon steel and the resulting influence on structural behavior (Baddoo & Francis, 2014; SCI, 2013). Meanwhile, ASCE-8 (ASCE, 2021), for the design of cold-formed austenitic, duplex and ferritic stainless steel structures, which is broadly aligned to AISI S100 (AISI, 2016), is also being substantially revised.

In this paper, stiffness reduction factors are derived to enable extension of the direct analysis method to the stability design of stainless steel structures. The accuracy of the proposed stiffness reduction method in predicting the capacity of austenitic, duplex and ferritic stainless steel members and frames is assessed relative to benchmark shell finite element results obtained second order inelastic analysis with imperfections – also referred to as geometrically and materially nonlinear analysis with imperfections (GMNIA). Comparisons are also made against a new method of design by second order inelastic analysis (GMNIA) with strain limits, which is due to be incorporated into AISC 370 (AISC, 2021; Walport, Gardner & Nethercot, 2021). The reliability of the design proposals is demonstrated through statistical analyses, and worked examples are presented to illustrate their application.

FINITE ELEMENT MODELLING

Both shell and beam finite element (FE) models are developed in this study; the shell FE models are utilized to generate benchmark results with which to assess the accuracy of the proposed design approach, while the beam FE models are used in the application of the stiffness reduction method. In this section, details of the FE modelling approach employed are presented. The FE models were developed using the general purpose FE software ABAQUS (ABAQUS, 2014) and validated against experimental results from the literature, as reported below.

Development of Benchmark Shell Finite Element Models

The generation of benchmark shell finite element results, obtained by means of second order inelastic analysis with imperfections (GMNIA), is described in this section. The four-noded reduced integration S4R shell element, from the ABAQUS (ABAQUS, 2014) element library, was employed herein to create all benchmark models, as successfully adopted in previous similar studies (Meng & Gardner, 2020; Kucukler, Gardner & Macorini, 2015; Bu & Gardner, 2019a). Both welded I-sections and cold-formed hollow sections were modeled, with the web depth and flange width subdivided into 12 elements to accurately capture local buckling and the spread of plasticity. The web plate was offset by half the thickness of each of the flanges such that overlapping of the flange and web plates was avoided. The

number of elements along the length of the members was defined such that the element aspect ratio was close to unity. The modified Riks method was used to trace the full load-deformation response of the modeled members and frames. Pin and roller support conditions were achieved through the coupling of the member end cross-section nodes to a master node, and in all cases the members were constrained out-of-plane along the flange centrelines at intervals close to the local buckling half-wavelength L_{el} (Fieber, Gardner & Macorini, 2019b). Note that, mirroring the approach taken in the development of the equivalent provisions in AISI S100, only cold-formed hollow sections are modeled herein. It is recommended that open cross-sections are considered in future research.

Geometric imperfections and residual stresses

In the benchmark models, an initial out-of-straightness in the form of a half-sine wave with a magnitude e_0 of 1/1000 of the member length L was assumed. For the frames, an initial out-of-plumbness of 1/500 of the frame height was assumed, as recommended in (AISC, 2016a), and applied as a notional load (H_{NL}). The geometric imperfections were incorporated into the models in the most unfavourable directions considering the applied loading and boundary conditions. Sinusoidal local plate imperfections were defined with an imperfection magnitude of 1/200 and 1/50 of the web height and half flange width, respectively, as recommended in EN 1993-1-5 (EN 1993-1-5, 2009), and a half-wavelength close to the elastic local buckling half-wavelength $L_{b,cs}$, calculated using the formulae set out in Fieber, Gardner & Macorini (2019b).

For the I-section models, the residual stress distribution for welded stainless steel I-sections developed by Yuan et al. (2014) was utilized, noting that stainless steel I-sections are predominately produced by welding. The residual stresses were modeled explicitly as an initial stress condition; corresponding plastic strains were also assigned (Kucukler, Xing & Gardner, 2020). An additional analysis step was included prior to loading to allow the residual stresses to equilibrate. Based on previous experimental and numerical findings (Ellobody & Young, 2005; Gardner & Nethercot, 2004; Jandera, Gardner & Machacek, 2008), residual stresses were not included in the hollow section FE models.

Material modeling

The stress-strain behavior of the modeled members and frames was described using the two-stage Ramberg-Osgood formulation (Arrayago, Real & Gardner, 2015; Mirambell & Real, 2000), as given by Eqs. (1) and (2):

$$\varepsilon = \frac{f}{E} + 0.002\left(\frac{f}{F_y}\right)^n \quad \text{for} \quad f \leq F_y \tag{1}$$

$$\varepsilon = 0.002 + \frac{F_y}{E} + \frac{f-F_y}{E_{Ty}} + \left(\varepsilon_u - 0.002 - \frac{F_y}{E} - \frac{F_u-F_y}{E_{Ty}}\right)\left(\frac{f-F_y}{F_u-F_y}\right)^m \quad \text{for} \quad F_y < f \leq F_u \tag{2}$$

where ε and f are the engineering strain and stress respectively, F_y is the yield (0.2% proof) stress, E is the Young's modulus, F_u is the ultimate stress, E_{Ty} is the tangent modulus at the yield (0.2% proof) stress, defined by Eq. (3), ε_u is the ultimate strain estimated as $\varepsilon_u = 1 - F_y/F_u$ for austenitic and duplex stainless steel and as $\varepsilon_u = 0.6(1 - F_y/F_u)$ for ferritic stainless steel, and n and m are the strain hardening exponents. In this study, typical grades of austenitic, duplex and ferritic stainless steel have been considered and the key material properties recommended in (AISC, 2021; ASCE, 2021) have been adopted, as summarised in Table 1.

$$E_{Ty} = \frac{E}{1+0.002n\frac{E}{F_y}} \tag{3}$$

Validation of shell finite element models

To validate the adopted shell finite element modeling approach, the 12 experiments of (Bu & Gardner, 2019b) on austenitic stainless steel I-section beam-columns were simulated. The testing comprised pin-ended members under uniaxial major or minor axis bending plus compression, with the initial loading eccentricities varied to provide a range of moment-to-axial load ratios. For the minor axis bending cases, the member slenderness L/r_y, where L is the member length and r_y is the radius of gyration about the minor axis, was equal to 95.9; for the major axis bending cases, the member slenderness L/r_x, where r_x is the radius of gyration about the major axis, was equal 57.0. The measured geometry and local and global imperfection amplitudes were incorporated into the FE models, along with the measured stress-strain response. Fig. 1 shows the experimental and numerical lateral deflection paths for five (three buckling about the major axis and two about the minor axis) of the 12 cases; the responses are consistently in close agreement. In terms of the failure load predictions, the mean FE-to-test ultimate load ratio was 0.99 and 0.98 for the six major and six minor cases, respectively, with corresponding COV values of 0.057 and 0.053, respectively. In addition to the accurate capacity predictions demonstrated herein, the adopted shell FE modeling approach has also been shown to provide accurate results in a number of previous studies (Meng & Gardner, 2020; Kucukler, Gardner & Macorini, 2015; Bu & Gardner, 2019a). The shell FE models are thus considered to be suitable for the generation of benchmark results against which to assess the design provisions proposed in this paper.

Development of Beam Finite Element Models

The 2-noded linear Timoshenko beam elements B31OS and B31, from the ABAQUS element library, were employed to create beam FE models with open and closed cross-sections, respectively, for implementation of the proposed design approach. Models were created of columns, beams, beam-columns and frames. In the developed frame models, the members were connected via fixed multi-point constraint ties at their ends providing full continuity. Results from the beam FE models were compared against those from shell FE models to ensure that the key member-level and frame-level behavioral features were accurately captured; this is demonstrated in Fig. 2, where load-deformation paths of an example austenitic stainless steel fixed based portal frame are compared. To account for the finite size of the rigid beam-to-column connections in the benchmark shell FE simulations, the member lengths in the beam FE models were shortened and rigid *MPC, Beam links were used to represent the connection region, as shown in Fig. 2a (Fieber, Gardner & Macorini, 2020). It can be seen that the shell and beam FE models provide essentially the same global response predictions.

DERIVATION OF STIFFNESS REDUCTION FACTORS FOR DESIGN BY SECOND ORDER ELASTIC ANALYSIS

In this section, stiffness reduction factors for the design of stainless steel structures by second order elastic analysis (GNA) are derived. The factors are derived in line with those for carbon steel members set out in AISC 360 (AISC, 2016b), but reflect the particular characteristics of stainless steel. The proposals are due to be incorporated into AISC 370 (AISC, 2021) and ASCE-8 (ASCE, 2021).

Stiffness Reduction Factor τ_b

The stiffness reduction factor τ_b accounts for the effects of yielding and residual stresses on the flexural stiffness of compression members; it should be applied by reducing the moment of inertia (second moment of area) of the columns and is a function of the level of axial loading.

Existing provisions for steel structures

In AISC 360 (AISC, 2016b), the stiffness reduction factor τ_b is given by Eq. (4) for steel structures and was derived from the Column Research Council (CRC) column strength curve (Lui & Ge, 2005), where P_r is the required axial compressive strength using LRFD or ASD load combinations and P_{ns} is the cross-section compressive strength; for nonslender sections $P_{ns} = F_y A_g$, where F_y is the yield stress and

A is cross-sectional area, and for slender sections $P_{ns} = F_y A_e$, where A_e is the effective cross-sectional area.

$$\tau_b = \begin{cases} 1.0 & \frac{P_r}{P_{ns}} \leq 0.5 \\ 4\left(\frac{P_r}{P_{ns}}\right)\left(1 - \frac{P_r}{P_{ns}}\right) & \frac{P_r}{P_{ns}} > 0.5 \end{cases} \quad (4)$$

The expression was obtained from the ratio of the inelastic to the elastic column buckling capacity (Yura, 1971; Liew, 1992), which can, broadly, be considered to follow the tangent modulus concept (Liew, White & Chen, 1994; Orbison, 1982; Liew, 1992; Deierlein, 2003; Lui & Ge, 2005). The reduction factor reflects the material behavior of carbon steel and the presence of residual stresses; for axial load levels less than half of the cross-section yield load, there is no stiffness reduction. Stiffness reduction commences beyond this value as plasticity develops at the outer fibres of the cross-section owing to the presence of residual stresses with peak values in compression assumed to be equal to one-half of the yield strength F_y (Orbison, 1982). The level of stiffness reduction increases under increasing axial load. Since τ_b is a function of the axial load level, it must be applied iteratively in the design process; the resulting forces and moments from the analysis are only true at the load level assumed in the calculation of τ_b. However, this step is often not needed because for steel design, τ_b only applies at relatively high axial load levels $P/P_{ns} > 0.5$ (Surovek-Maleck & White, 2004a). Since Eq. (4) i.e. the CRC column curve does not consider member out-of-straightness in its derivation, allowance for these bow imperfections is needed either through member checks or through direct modelling in the analysis.

Development of new provisions for stainless steel structures

A stiffness reduction function for stainless steel compression members to account for the influence of plasticity $\tau_{b,m}$ can be directly derived from the Ramberg-Osgood expression (Eq. (1)). Defining the stiffness reduction factor due to material nonlinearity as the ratio of the tangent to the Young's modulus, $\tau_{b,m} = E_t/E$, where $E_t = df/d\varepsilon$ and $f = P/A$, the following expression is obtained:

$$\tau_{b,m} = \frac{1}{1+0.002n\frac{E}{F_y}\left(\frac{P_r}{P_{ns}}\right)^{n-1}} \quad (5)$$

where P_r is the required axial compressive strength using LRFD or ASD load combinations and P_{ns} is the cross-section compressive strength.

To consider the additional contribution to stiffness reduction of residual stresses, expressions for τ_b for buckling about the major and minor axis were calibrated against the major (x-x) and minor (y-y) axis

tangent flexural stiffness reduction obtained from finite element models of stainless steel welded I-section stub columns with residual stresses. A W8×31 cross-section, divided into n = 1440 monitoring areas (each of area A_i, distance to centroid in the x and y direction y_i and x_i, and tangent stiffness E_i), was subjected to pure axial compression. For each axis of buckling (x-x and y-y), the numerical stiffness reduction factor $\tau_{b,FE}$ was calculated through the summation of the contribution of each element i to the flexural stiffness, as given by Eqs. (6) and (7).

$$\tau_{b,x,FE} = \frac{\sum_{i=1}^{n} E_{t,i} A_i y_i^2}{\sum_{i=1}^{n} E A_i y_i^2} \tag{6}$$

$$\tau_{b,y,FE} = \frac{\sum_{i=1}^{n} E_{t,i} A_i x_i^2}{\sum_{i=1}^{n} E A_i x_i^2} \tag{7}$$

The proposed stiffness reduction factor τ_b, accounting for the combined effects of material nonlinearity and residual stresses, was derived on the basis of Eq. (5), but with the strain hardening exponent n modified to an effective strain hardening exponent n_{eff} to allow for the influence of residual stresses by calibration against the results of Eqs. (6) and (7) for the different axes of buckling. The proposed expression for τ_b is given by Eq. (8) and illustrated in Fig. 3, while the values of the effective strain hardening exponents n_{eff} are presented in Table 2.

$$\tau_b = \frac{1}{1+0.002 n_{eff} \frac{E}{F_y} \left(\frac{P_r}{P_{ns}}\right)^{n_{eff}-1}} \tag{8}$$

The differing values of n_{eff} for the different buckling axes reflect the fact that the flexural stiffness is reduced more severely for the minor axis than the major axis due to the more detrimental influence of the compressive residual stresses at the flange tips, as seen in Fig. 3. In the case of rectangular hollow structural sections (HSS), since the residual stresses are small, the ratio of the tangent flexural stiffness to the initial elastic flexural stiffness can be assumed to equal to $\tau_{b,m}$ (i.e. n_{eff} equal to n). To retain the same demarcation between cross-sections as the AISC 370 flexural buckling curves (see Table 4), the stiffness reduction function for welded box sections and round HSS is taken equal to that for I-sections buckling about the major axis.

Since n_{eff} is a function of n, the varying degrees of roundedness of the stress-strain curves for the different grades of stainless steel (with the typical austenitic grade 304, duplex grade S32101 and ferritic grade 41OS studied herein) is reflected in τ_b, as shown in Fig. 4. Alongside the proposed stiffness reduction factors, the carbon steel stiffness reduction factor, given by Eq. (4), is also presented in Fig. 4. It can be seen that, unlike in AISC 360 (AISC, 2016b), the stiffness reduction for stainless steel

commences from the onset of loading. This stems from the stiffness reduction function being based on the Ramberg-Osgood material model, which features a contribution from the nonlinear term ($0.002(f/F_y)^n$ in Eq. (1)) at all stress levels, despite the actual material response being purely elastic in the initial stages. Nonetheless, the early onset of stiffness reduction is an accurate reflection of the inherent rounded stress-strain response of stainless steel, exacerbated by the influence of the residual stresses. The greatest reduction at low to moderate axial load levels occurs for austenitic stainless steel, mirroring the low limit of proportionality and the low value of the strain hardening exponent n, resulting in the highest degree of nonlinearity of stress-strain response among the three main families of stainless steel.

In ASCE-8-20 (ASCE, 2021), for the design of cold-formed stainless steel structural members, a single column curve, corresponding to that for the minor axis buckling of I-sections in AISC 370, is provided; the value of n_{eff} for this case is therefore proposed for inclusion in ASCE-8 (ASCE, 2021), as given in Table 2, and presented in Fig. 5 for the typical grades of stainless steel.

Amplified Notional Load Approach

Application of the stiffness reduction method is inherently an iterative process; the stiffness reduction factors τ_b are calculated at the load level of interest and the results of the subsequent second order analysis (GNA) are only valid at that same load level. An alternative, simpler approach that avoids the need for iteration is to replace the use of τ_b factors (i.e. by setting τ_b = 1.0 for all members) with the application of additional notional horizontal loads (H_{ANL}). The enhanced notional loads are designed to account indirectly for the effect of the spread of plasticity and residual stresses on the global response of the structure. However, since the additional notional loads impact the behavior of the full structure, rather than just the heavily loaded members, overly conservative resistance predictions can result when P–Δ effects are significant.

Existing provisions for steel structures

In AISC 360 (AISC, 2016b), additional notional loads of magnitude 0.001 of the total factored gravity loads acting at each story of structural frames are defined.

Development of new provisions for stainless steel structures

The stiffness reduction factors τ_b derived for stainless steel herein are more severe than those for carbon steel, reflecting the earlier initiation of yielding of the material. A commensurate increase in the additional notional horizontal load (H_{ANL}) from 0.001 to 0.002 of the total factored gravity load applied at each story of structural frames is therefore proposed for inclusion in both AISC 370 and ASCE-8 for stainless steel design. The appropriateness of this proposal is demonstrated in subsequent sections (see also Tables 7, 9, 11-13 and Figures 6, 8, 11 and 13).

Stiffness Reduction Factor τ_g

The general stiffness reduction factor τ_g accounts for the reduction in member stiffness due to the development and spread of plasticity; it is applied to all members in the structure by uniformly reducing the Young's and shear moduli. For structures that are governed by elastic buckling, the τ_g factor results in design strengths approximately equal to τ_g times the elastic stability limit.

Existing provisions for steel structures

In AISC 360, a reduction factor τ_g of 0.8 is prescribed to account for the reduction in stiffness due to plasticity. The value of 0.8 was derived from benchmark studies presented by (Surovek-Maleck, 2001; Surovek-Maleck & White, 2004b) considering a 0.9 factor for strong-axis beam-column strength predictions and its multiplication by ϕ (0.9). Note that these studies showed that a value of 0.7 (0.8ϕ) is required for weak axis bending. For slender members, where τ_b is equal to unity, the 0.8 factor results corresponds approximately to the margin of safety implied in the column curves i.e. $0.8 = 0.9 \times 0.877$ (Deierlein, 2003; Surovek-Maleck & White, 2004a).

Development of new provisions for stainless steel structures

In this study, τ_g has been calibrated against benchmark results from the nonlinear shell finite element analysis of a series of stainless steel columns, beams, beam-columns and portal frames, considering different cross-section shapes and a range of slenderness values, axial load-to-bending ratios and column-to-beam stiffness ratios for the frames. Based on an extensive range of comparisons, presented in subsequent sections, a value of $\tau_g = 0.7$ is proposed, as given in Table 2. Note that a single value of τ_g, as employed for carbon steel in AISC 360, is deemed suitable for all grades of stainless steel, with the value of 0.7 being roughly equal to the minimum flexural buckling coefficient β_2 (see Table 4) that controls the flexural buckling strength of slender columns.

In ASCE-08 (ASCE, 2021), for the design of cold-formed stainless steel structural members, a stiffness reduction factor τ_g equal to 0.9 is recommended, as given in Table 2. The difference between the proposed value of τ_g for AISC 370 and ASCE-08 reflects the different cross-section force-moment interaction equation, the different column buckling curves and the different moment capacities between the two codes. Note that while $\tau_g = 0.9$ is larger than the corresponding value of 0.8 used in AISC 360 for steel, since τ_b drops below unity at low axial load levels for stainless steel, unlike the case for steel where $\tau_b = 1.0$ up to $P = 0.5P_y$, the overall stiffness reduction (i.e. $\tau_g\tau_b$) is similar between the two materials for slender members (i.e. low axial load levels).

DESIGN BY SECOND ORDER ELASTIC ANALYSIS

In design by second order elastic analysis (GNA), the stiffness reduction factors are employed to recognise the influence of plasticity and residual stresses. The resistance of the members must be subsequently verified either by member buckling checks or, if initial bow imperfections are included in the members of the analysed structure, cross-section checks. In all cases, an out-of-plumbness ratio of 1/500 must be either directly modeled or applied as a set of equivalent notional loads of magnitude equal to 0.002 times the total gravity load applied at each story of the structure (H_{NL}). In Table 3, four options, referred to as Design Cases 1, 2, 3 and 4 and abbreviated to DC1, DC2, DC3 and DC4, for design by second order elastic analysis (geometrically nonlinear analysis, GNA – DC1, DC2; geometrically nonlinear analysis with imperfections GNIA – DC3, DC4) are detailed. Design Cases 1 and 2 require member checks, while Design Cases 3 and 4 include member imperfections and therefore resistances can be verified with cross-section checks only. To take account of the additional capacity due to strain hardening, Design Case 4 utilizes the continuous strength method given in Appendix 2 of AISC 370 and Section 6 of ASCE-8.

Member Buckling Checks

In Design Cases 1 and 2, flexural buckling is accounted for through member buckling checks and the required compressive strength P_c is taken as the nominal compressive strength equal to the critical stress F_{cr} multiplied by the cross-section area A. In this study, the critical stress F_{cr} has been determined using the revised column curves included in AISC 370 (AISC, 2021), and given by Eqs. (9)-(11):

$$F_{cr} = F_e \quad \text{for} \quad \frac{L}{r} \leq \beta_0 \sqrt{\frac{E}{F_y}} \tag{9}$$

$$F_{cr} = 1.2\left(\beta_1^{\left(\frac{F_y}{F_e}\right)^{\alpha}}\right)F_y \quad \text{for} \quad \beta_0\sqrt{\frac{E}{F_y}} < \frac{L}{r} \leq 5.62\sqrt{\frac{E}{F_y}} \tag{10}$$

$$F_{cr} = \beta_2 F_e \quad \text{for} \quad \frac{L}{r} > 5.62\sqrt{\frac{E}{F_y}} \tag{11}$$

where F_y is the yield stress, E is the modulus of elasticity, F_e is the elastic buckling stress given by Eq. (12):

$$F_e = \frac{\pi^2 E}{\left(L/r\right)^2} \tag{12}$$

where L is the effective member length, equal to the laterally unbraced length of the member multiplied by the effective length factor K, r is the radius of gyration, and α, β_0, β_1 and β_2 are the flexural buckling coefficients, as defined in Table 4 (Meza, Baddoo & Gardner, 2021). Note that the effective length for flexural buckling of all members is taken as the unbraced length herein i.e. $K = 1$ (AISC, 2021).

Unlike in AISC 360, these curves take account of the varying influence of residual stresses by differentiating between the different axes of buckling and cross-section shapes, in a similar manner to EN 1993-1-4 (EN 1993-1-4:2006 + A1:, 2015; Afshan *et al.*, 2015). Additionally, the curves include a plateau, as defined by Eq. (9), for members with low slenderness L/r; this recognises that the strength of short stainless steel members exceed the yield load as a result of strain hardening.

In ASCE-8, a single flexural buckling curve is given for all cross-section shapes. The curve is the same as that given in AISC 370 for the minor axis flexural buckling of I-section members but with an allowance for capacities in excess of the yield load for members with low slenderness (i.e. members satisfying $L/r \leq \beta_0\sqrt{E/F_y}$).

The flexural strength of members should be calculated considering the limit state of yielding, local buckling and lateral-torsional buckling. For the in-plane bending of beams with compact cross-sections, only the limit state of yielding needs to be considered and the nominal flexural strength M_n is given as F_yZ, where Z is the plastic section modulus about the axis of bending. Note that stainless steel exhibits substantial levels of strain hardening; in strength governed cases capacities can far exceed the plastic moment capacity M_p. This benefit is captured in the continuous strength method, which features in the provisions of both AISC 370 and ASCE-8, as discussed in the following section.

For combined loading, the nonlinear interaction curve given by Eqs. (13) and (14), is employed in both AISC 360 (AISC, 2016b) and 370 (AISC, 2021), while in ASCE-8 (ASCE, 2021) the linear interaction curve given by Eq. (15) is used.

$$\frac{P_r}{P_n} + \frac{8}{9}\frac{M_r}{M_n} \leq 1.0 \quad \text{for} \quad \frac{P_r}{P_n} \geq 0.2 \tag{13}$$

$$\frac{P_r}{2P_n} + \frac{M_r}{M_n} \leq 1.0 \quad \text{for} \quad \frac{P_r}{P_n} < 0.2 \tag{14}$$

$$\frac{P_r}{P_n} + \frac{M_r}{M_n} \leq 1.0 \tag{15}$$

where P_r and M_r are the required compressive and flexural strengths, respectively, and P_n and M_n are the nominal compressive and flexural strengths, respectively.

For Design Cases 1 and 2, for the example case of members with compact cross-sections, the resistances are therefore verified (according to AISC 370 design) using Eqs. (16) and (17).

$$\frac{P_r}{F_{cr}A} + \frac{8}{9}\frac{M_r}{F_yZ} \leq 1.0 \quad \text{for} \quad \frac{P_r}{F_{cr}A} \geq 0.2 \tag{16}$$

$$\frac{P_r}{2F_{cr}A} + \frac{M_r}{F_yZ} \leq 1.0 \quad \text{for} \quad \frac{P_r}{F_{cr}A} < 0.2 \tag{17}$$

Since the influence of the spread of plasticity and residual stresses are accounted for through stiffness reduction and the influence of out-of-plumbness on the structural response is considered through direct modeling or by the application of notional horizontal loads in a second order analysis, unbraced member lengths are used in the member checks (Deierlein, 2003; Kucukler, Gardner & Macorini, 2014).

Cross-section Checks

If member bow imperfections are included in the structural model, member instability is directly captured in the second order analysis and only cross-section strength checks are required to verify the capacity of the structure. This method is set out in Appendix 1 of both AISC 360 (AISC, 2016b) and 370 (AISC, 2021). The cross-section strength check is performed using Eqs. (13) and (14), but with the nominal compressive strength of the member P_n taken as the cross-section compressive strength F_yA, where A is the cross-section area, or as F_yA_e for members with slender elements, where A_e is the effective area of the cross-section; the resulting cross-section interaction curve is given by Eqs. (18) and (19) for the case of compact cross-sections. This method is referred to herein as Design Case 3 – see Table 3.

$$\frac{P_r}{F_yA} + \frac{8}{9}\frac{M_r}{F_yZ} \leq 1.0 \quad \text{for} \quad \frac{P_r}{F_y} \geq 0.2 \tag{18}$$

$$\frac{P_r}{2F_yA} + \frac{M_r}{F_yZ} \leq 1.0 \quad \text{for} \quad \frac{P_r}{F_yA} < 0.2 \tag{19}$$

Note that in AISC 360 (AISC, 2016b), the use of additional notional loads in place of stiffness reduction through τ_b is not permitted with the method described in this sub-section; the same restriction is applied in AISC 370 (AISC, 2021).

Continuous strength method

The continuous strength method (CSM) is a deformation based design approach that enables a rational exploitation of the spread of plasticity, strain hardening and element interaction in the design of stainless steel cross-sections (Afshan & Gardner, 2013; Gardner, 2008). The method is set out in Appendix 2 of AISC 370 (and is also included for the calculation of flexural strength in Chapter 6 of ASCE-8), and can be used for the verification of members with initial bow imperfections through second order elastic analysis (GNIA) plus CSM cross-section checks. This method of design is referred to as Design Case 4 – see Table 3. The same interaction equations (i.e. Eqs. (13) and (14)) apply, but with the CSM cross-section resistances in compression $P_{n,csm}$ and bending $M_{n,csm}$ used in place of P_n and M_n to give:

$$\frac{P_r}{P_{n,csm}} + \frac{8}{9}\frac{M_r}{M_{n,csm}} \leq 1.0 \quad \text{for} \quad \frac{P_r}{P_{n,csm}} \geq 0.2 \tag{20}$$

$$\frac{P_r}{2P_{n,csm}} + \frac{M_r}{M_{n,csm}} \leq 1.0 \quad \text{for} \quad \frac{P_r}{P_{n,csm}} < 0.2 \tag{21}$$

where $P_{n,csm}$ is given by:

$$P_{n,csm} = \frac{\varepsilon_{csm}}{\varepsilon_y} F_y A_g \quad \text{for} \quad \frac{\varepsilon_{csm}}{\varepsilon_y} < 1.0 \tag{22}$$

$$P_{n,csm} = F_{csm} A_g \quad \text{for} \quad \frac{\varepsilon_{csm}}{\varepsilon_y} \geq 1.0 \tag{23}$$

and $M_{n,csm}$ is given by:

$$M_{n,csm} = \frac{\varepsilon_{csm}}{\varepsilon_y} M_y \quad \text{for} \quad \frac{\varepsilon_{csm}}{\varepsilon_y} < 1.0 \tag{24}$$

$$M_{n,csm} = M_p \left(1 + \frac{E_{sh}}{E}\frac{S}{Z}\left(\frac{\varepsilon_{csm}}{\varepsilon_y} - 1\right) - \left(1 - \frac{S}{Z}\right)/\left(\frac{\varepsilon_{csm}}{\varepsilon_y}\right)^{\alpha}\right) \quad \text{for} \quad \frac{\varepsilon_{csm}}{\varepsilon_y} \geq 1.0 \tag{25}$$

where F_{csm} is the CSM design stress, as given by Eq. (26), ε_y is the yield strain equal to F_y/E, E_{sh} is the strain hardening modulus, as given by Eq. (27), where C_2 is equal to 0.16 for austenitic and duplex stainless steel and 0.45 for ferritic stainless steel, M_y is the elastic moment capacity, M_p is the plastic moment capacity, S is the elastic section modulus, Z is the plastic section modulus, and ε_u is the ultimate

388 tensile strain, estimated as $\varepsilon_u = 1 - F_y/F_u$ for austenitic and duplex stainless steel and as $\varepsilon_u = 0.6(1 -$
389 $F_y/F_u)$ for ferritic stainless steel.

390 $$F_{csm} = F_y + E_{sh}\varepsilon_y\left(\frac{\varepsilon_{csm}}{\varepsilon_y} - 1\right) \quad \text{for} \quad \frac{\varepsilon_{csm}}{\varepsilon_y} \geq 1.0 \tag{26}$$

391 $$E_{sh} = \frac{F_u - F_y}{C_2\varepsilon_u - \varepsilon_y} \tag{27}$$

392 The ratio $\varepsilon_{csm}/\varepsilon_y$ defines the maximum strain that the cross-section can tolerate ε_{csm} as a multiple of the
393 yield strain, and is obtained from Gardner, Wang & Liew (2011):

394 $$\frac{\varepsilon_{csm}}{\varepsilon_y} = \frac{0.25}{\lambda_l^{3.6}} \leq \min\left(\Lambda, \frac{C_1\varepsilon_u}{\varepsilon_y}\right) \quad \text{for} \quad \lambda_l \leq 0.68 \tag{28}$$

395 $$\frac{\varepsilon_{csm}}{\varepsilon_y} = \left(1 - \frac{0.222}{\lambda_l^{1.05}}\right)\frac{1}{\lambda_l^{1.05}} \quad \text{for} \quad 0.68 < \lambda_l \leq 1.6 \tag{29}$$

396 Eqs. (28) and (29) are applicable to non-slender and slender cross-sections, respectively, where λ_l
397 (denoted $\bar{\lambda}_{p,cs}$ in prEN 1993-1-4 (prEN 1993-1-4, 2020)) is the cross-sectional slenderness, C_1 is equal
398 to 0.1 for austenitic and duplex stainless steels and 0.4 for ferritic stainless steels (Afshan & Gardner,
399 2013; Bock, Gardner & Real, 2015), and Λ (denoted Ω in EN 1993-1-4 (prEN 1993-1-4, 2020)), is a
400 project specific design parameter defining the maximum allowable level of plastic deformation (Fieber,
401 Gardner & Macorini, 2019a). For design by elastic analysis with stiffness reduction, Λ is equal to 5.

402 **DESIGN BY SECOND ORDER INELASTIC ANALYSIS**

403 The most accurate representation of the behavior of a structure, leading to the most accurate design
404 method, is achieved through the use of second order inelastic analysis – also referred to as geometrically
405 and materially nonlinear analysis with imperfections (GMNIA). In this approach, the influence of the
406 material nonlinearity on the structural response is directly modeled through the definition of the full
407 stress-strain curve of the material in the second order analysis. Plastic hinges do not provide an accurate
408 reflection of the gradual spread of plasticity seen in stainless steel structures. It is therefore necessary
409 to account for the zones of plasticity by directly modeling the nonlinear material stress-strain response
410 in a plastic zone, also known as distributed plasticity or fibre, analysis (Walport *et al.*, 2019). A new
411 method for the design of stainless steel structures by second order inelastic analysis with imperfections
412 (GMNIA), performed using beam finite element analysis is included in Appendix 1 of AISC 370 (AISC,
413 2021; Walport, Gardner & Nethercot, 2021). This corresponds to Design Case 5 (DC5) in Table 3. In
414 this design method, accurate material modeling is ensured through use of the two-stage Ramberg-

Osgood expression, while cross-section strength checks are replaced by the application of strain limits. The strain limits depend on the slenderness of the cross-section. Consequently, cross-section slenderness dependent levels of spread of plasticity, moment redistribution and strain hardening can be exploited, in a consistent and rational manner enabling accurate predictions of the resistance of structural systems. The strain limits are taken from the CSM, as given by Eqs. (30) and (31), where f is the maximum stress level in the cross-section and n is the strain hardening exponent of the Ramberg–Osgood material model. Note that these Equations differ from the CSM base curve given by Eqs. (28) and (29) to account for the difference between the bilinear and rounded stress-strain curves. Also, a stricter limit is placed on the maximum value of λ_l (1.0 instead of 1.6) for system level design by second order inelastic analysis (GMNIA).

$$\frac{\varepsilon_{csm}}{\varepsilon_y} = \frac{0.25}{\lambda_l^{3.6}} + \frac{0.002}{\varepsilon_y} \quad \text{but} \quad \frac{\varepsilon_{csm}}{\varepsilon_y} \leq \Lambda \quad \text{for} \quad \lambda_l \leq 0.68 \tag{30}$$

$$\frac{\varepsilon_{csm}}{\varepsilon_y} = \left(1 - \frac{0.222}{\lambda_l^{1.05}}\right) \frac{1}{\lambda_l^{1.05}} + \frac{0.002\left(f/f_y\right)^n}{\varepsilon_y} \quad \text{for} \quad 0.68 < \lambda_l \leq 1.0 \tag{31}$$

To allow for the beneficial influence of moment gradients, the maximum compressive strains output from the second order inelastic analysis (GMNIA) at each cross-section are averaged over the elastic local buckling half-wavelength L_{el}, denoted $L_{b,cs}$ in prEN 1993-1-4 (prEN 1993-1-4, 2020), (Fieber, Gardner & Macorini, 2019a; Walport, Gardner & Nethercot, 2021). The elastic local buckling half-wavelength of the cross-section L_{el} may be obtained numerically or using the simplified expressions given in Fieber, Gardner & Macorini (2019b) – the magnitude of the elastic local buckling half-wavelength will normally be in the region of the cross-section plate widths. The value of L_{el} also defines the maximum length of the beam elements to be utilized in the analysis.

Initial geometric imperfections and residual stresses must be considered in the analysis and can be modeled as either (1) a member bow imperfection of magnitude L/1000, where L is the member length, plus residual stresses, or (2) an equivalent member imperfection that accounts for the combined influence of geometric imperfections and residual stress, as given by Eq. (32), where e_0 is the bow imperfection magnitude, α_{eq} is the imperfection factor (prEN 1993-1-4, 2020), the values of which are given in Table 5 for common cases, and β = 1/150 (Walport, Gardner & Nethercot, 2020).

$$\frac{e_0}{L} = \alpha_{eq}\beta \quad \text{but} \quad \frac{e_0}{L} \geq \frac{1}{1000} \tag{32}$$

Through this method of design by second order inelastic analysis with imperfections (GMNIA), failure of a system occurs either at the load level at which the CSM strain limit is reached, or, in stability dominated cases, at the load level at which the analysis reaches a peak (Walport, Gardner & Nethercot, 2021).

ASSESSMENT OF PROPOSALS FOR MEMBER DESIGN

The accuracy and reliability of the developed recommendations for the design of stainless steel columns, beams and beam-columns is assessed in this section with respect to the benchmark shell FE ultimate loads determined using GMNIA.

Results

In this section, the results of the elastic and inelastic design methods, as outlined in Table 3, are compared against benchmark shell FE results for austenitic, duplex and ferritic stainless steel columns, beams and beam-columns. Note that Design Case 2 is not considered in this section as this only relates to analyses at system level. Design Cases 1, 3 and 4 incorporate the developed stiffness reduction factors combined with elastic analysis, while Design Case 5 utilizes inelastic analysis. These are summarised as follows - DC1: GNA + τ_g + τ_b + member check, DC3: GNIA + τ_g + τ_b + cross-section check, DC4: GNIA + τ_g + τ_b + cross-section check + CSM end points and DC5: GMNIA (equivalent imperfections) + CSM strain limits.

Table 6 presents the results from the austenitic, duplex and ferritic stainless steel W8×31 and SHS8×8×3/8 cross-section beam-columns considered in this study. Five member slenderness values L/r (20, 40, 80, 120 and 160), where L is the member length and $r = \sqrt{I/A}$ is the radius of gyration with I being the moment of inertia (second moment of area) and A the cross-sectional area, and three bending moment distributions (BMD) along the member length (BMD 1: $\psi = 1$, BMD 2: $\psi = 0$, BMD 3: $\psi = -0.5$), achieved by changing the ratio of applied end moments $\psi = M_2/M_1$, where M_1 and M_2 are the applied end moments, were considered. Note that for the duplex stainless steel members, which have higher strengths than other grades and hence are more strongly influenced by buckling effects for a given geometry, only the practical L/r ratios of 20, 40 and 80 were considered. It can be seen that for all grades of stainless steel, the proposed stiffness reduction factors τ_b and τ_g result in generally safe sided average capacity predictions compared with the benchmark shell FE results (ranging between 27% on the safe side to 6% on the unsafe side).

Fig. 6 shows a comparison between the capacity predictions of the austenitic stainless steel W-section columns, beams and beam-columns subjected to major axis bending obtained using the four design approaches and the benchmark shell FE results. The results are presented in terms of the radial error versus the radial angle, as defined in Fig. 7, where R_{FE} and R_d are the radial distances measured from the origin to the data points in M–N space determined from the benchmark FE model and the considered design approach, respectively. Values of radial error larger than unity indicate safe-sided predictions. A radial angle of 0° corresponds to pure bending while a radial angle of 90° corresponds to pure compression. The level of scatter in the predictions (either side of the mean) of Design Cases 1 to 4 is similar to that obtained using the equivalent rules for carbon steel structures (Surovek-Maleck & White, 2004b; Ziemian & Wang, 2019). The scatter is related, in part, to the use of a uniform τ_g and the lack of consideration given to the influence of the shape of the bending moment diagram on the development of the plasticity (Kucukler, Gardner & Macorini, 2016); this can be seen in the results presented in Table 6 and Fig. 6, which become increasingly conservative with increasing bending moment gradient i.e transitioning from BMD 1 to 3. Additionally, while the significant strain hardening effects associated with stainless steel are fully captured through accurate material modeling in the benchmark shell FE results, they are essentially disregarded in Design Cases 1-3 and partially reflected through the use of the CSM end points in Design Case 4. From Fig. 6, it can be seen that when the radial angle is between 0° and 50°, there are a number of capacity predictions on the unsafe side. This is because, for members subjected to high levels of bending, particularly those of stocky proportions, the real degree of stiffness reduction is greater than that obtained using the proposed design approach, but applying more severe stiffness reduction (i.e. a lower value of τ_g) would render the capacity predictions of slender members and those dominated by compression very conservative. A balance has therefore been struck, with τ_g = 0.7 for AISC 370 and τ_g = 0.9 for ASCE-8, the appropriateness of which is demonstrated in the reliability analyses presented in the following sub-section (see also Table 6).

Design Case 5, in which the full nonlinear stress-strain response is explicitly modeled and the influence of moment gradients is captured through strain averaging provides very accurate and consistent results for all three loading arrangements. Note, in particular, that the standard deviation of the radial error is considerably lower for DC5 than all cases of design by second order elastic analysis (GNA/GNIA), ranging between 0.03 and 0.07, compared with 0.04 and 0.21 for DC1-4 – see Table 6.

Reliability Analysis

The safety of the proposed structural design provisions are assessed in this sub-section. Values of the resistance factor ϕ have been calculated from Eq. (33) for each dataset, based on a target reliability index β equal to 2.6 and a dead-to-live load ratio of 1:3 (SCI, 2013; Bartlett *et al.*, 2003; Lin, Yu & Galambos, 1992). The recommended value for the resistance factor ϕ is 0.9 and this is therefore taken as the target value in the present study.

$$\phi = \frac{1.481 M_m F_m P_m}{\exp\left(\beta \sqrt{V_R^2 + V_Q^2}\right)} \tag{33}$$

In Eq. (33), M_m, F_m and P_m are the mean values of the random variables associated with material properties, cross-section geometry and design rule assumptions, respectively, and V_R and V_Q are the coefficient of variation of the load effect Q and resistance R, respectively. The coefficient of variation of the resistance V_R is calculated from Eq. (34), where V_M, V_F and V_P are the coefficients of variation associated with the uncertainties in material properties, fabrication and design rule assumptions, respectively. The parameters considered in this study are given in Table 7 (Afshan *et al.*, 2015; Baddoo, Meza & Gardner, 2020).

$$V_R = \sqrt{V_M^2 + V_F^2 + V_P^2} \tag{34}$$

The calculated required ϕ factors are presented in Table 6, where it can be seen that all values are greater than the value of 0.9 included in AISC 370, and therefore the target reliability is achieved. In some cases, the ϕ factors are well in excess of 0.9 (with a maximum ϕ value of 1.24), suggesting over-conservatism. However, as well as achieving desirable ϕ factor values, weight was also given to ensuring that the mean capacity predictions for the different groups considered were not too much on the unsafe side (i.e. with an average ε ratio below unity) and similarly, that capacities of individual members were not excessively over-predicted. It should also be noted that stainless steels have high over-strength factors (see Table 7) which, in the AISC reliability analysis framework, uniformly benefit all members, regardless of their slenderness and the applied loading, while in reality, the benefit of overstrength dissipates with increasing slenderness as instability dominates. Overall, the attained ϕ factors are similar to those achieved in the reliability assessment of the other design provisions in AISC 370 (AISC, 2021), as outlined in DG27 (SCI, 2013). A resistance factor of 0.9 is therefore recommended.

APPLICATION OF METHOD TO STRUCTURAL FRAMES

In this section, the accuracy of all five design cases, including Design Case 2 (GNIA + τ_g + H_{ANL} + member check), for the in-plane design of stainless steel frames is assessed. As previously outlined, an alternative to applying the stiffness reduction factors τ_b, which is an iterative process, is to impose additional notional horizontal loads (H_{ANL}) of magnitude 0.002 of the total factored gravity load applied at that story of the structure. Fig. 8 shows a comparison of the results of a one bay fixed based austenitic stainless steel (F_y = 205 N/mm^2, E = 193000 N/mm^2) portal frame obtained from (1) benchmark shell FE GMNIA and (2) Design case 2 i.e. second order elastic analysis (GNA) with no member imperfections modeled, a stiffness reduction of τ_g applied to all members, a notional horizontal load of magnitude 0.002 times the vertical load (to represent out-of-plumbness), an additional notional horizontal load (H_{ANL}) of the same magnitude and member checks, in which P_{ns} and M_p correspond to the column buckling resistance and major axis plastic bending moment resistance of the columns, respectively. The ratio of the column height L_c to beam length L_b was fixed at 1:3, resulting in a ratio of the flexural stiffness of the columns to that of the beams of $G_R = (I_c/L_c)/(I_b/L_b) \approx 1.0$, while three column lengths were modeled to achieve a range of member slenderness values L/r. It can be seen in Fig. 8 that the stiffness reduction method with additional notional loads (H_{ANL}) results in safe sided predictions in all cases. The level of conservatism increases as the bending moment increases. This is the result of two limitations to the approach: (1) the additional notional load (H_{ANL}) does not consider the variation in axial load level between members, as captured in τ_b, and therefore effectively applies to members on the basis of their contribution, through their elastic stiffnesses, to the lateral stability of the frame and (2) the member check limits the bending capacity to the plastic moment capacity M_p, while the benchmark shell FE model captures the beneficial influence of strain hardening.

Vogel Frame

In this sub-section, the second order elastic (DC1 to DC4 – GNA/GNIA) and inelastic (DC5 – GMNIA) design methods presented herein are applied to the six-story Vogel frame (Vogel, 1985), as shown in Fig. 9, with austenitic stainless steel material properties (E = 193000 N/mm^2, F_y = 205 N/mm^2, F_u = 515 N/mm^2, n = 7). The benchmark frame response was determined using second order inelastic analysis with imperfections (GMNIA - L/1000 + residual stresses) using beam finite elements. Beam elements were deemed to be acceptable in the benchmark model since the behavior of the Vogel frame is controlled by overall stability, rather than cross-section strength, and a very similar result would

therefore be expected from a shell FE simulation. Fig. 10 shows the load-deformation path of the Vogel frame; for validation of the modeling approach, a GMNIA of the Vogel frame was also carried out using the original steel material properties (E = 205000 N/mm^2, F_y = 235 N/mm^2) and plotted alongside the original response presented by Vogel (Vogel, 1985) – a close match can be observed in Fig. 10.

The ultimate design load factors for the Vogel (Vogel, 1985) frame α_{DC}, calculated as the load level for which the utilisation ratio of the critical member reaches unity for the different design cases (DC1-5), along with benchmark ultimate load factor obtained from GMNIA, are presented in Table 8 and shown in Fig. 11. The α_{DC} values were determined through iteration for Design Cases 1, 3 and 4, with the stiffness reduction factors recalculated considering the first-order member forces at the load factor α_{DC}. The capacity predictions for Design Cases 1 to 4 are safe sided and are of similar accuracy to those determined for the equivalent frame in carbon steel by Kucukler, Gardner & Macorini (2016) – average predicted-to-FE capacity ratios of 0.99 to 1.07 compared with 1.02 and 1.06 for the direct analysis method (equivalent to DC1) and notional load method (equivalent to DC2), respectively, for carbon steel. The behavior of the frame is best represented by DC5 since all material and geometric nonlinearities are explicitly modeled, leading to the most accurate prediction of both the distribution of internal forces and moments and structural capacity. Note that the load-deformation path of DC5 differs from the benchmark response due to the use of equivalent geometric imperfections in DC5 (Eq. (32)) instead of the explicit modeling of both geometric imperfections (L/1000) and residual stresses in the benchmark model.

The stiffness reduction factors τ_b for Design Cases 1-4 at the ultimate system load (i.e. when the critical member had a utilisation equal to unity) for each member in the Vogel frame are presented in Table 9. It can be seen that the middle columns of each story have the lowest stiffness reduction factors, representing the highest level of plasticity. Note that τ_b is only applied to the flexural stiffnesses (i.e. by reducing the second moments of areas) of the columns while τ_g = 0.7 is applied uniformly to all members through the reduction of the Young's modulus E and shear modulus G.

As well as the ultimate design load, it is important to consider the accuracy of the prediction of the distribution of forces and moments within the frame. Table 10 presents a comparison of the maximum normalised bending moments within the members of the Vogel frame determined at the ultimate system loads for the five design cases considered. The maximum bending moment in each member at the ultimate system load M_{DC} is presented normalised by the plastic moment capacity M_p (i.e. M_{DC}/M_p) of

588 the member, as well as by the corresponding bending moment obtained from the benchmark GMNIA
589 M_{GMNIA} (i.e. M_{DC}/M_{GMNIA}). The bending moments are generally well predicted, with the largest
590 discrepancies arising in members with relatively low bending moments at failure. For example, in DC1,
591 the maximum M_{DC}/M_{GMNIA} value of 1.23 occurs in member C26 which has a M_{DC}/M_p value of 0.09,
592 while the minimum M_{DC}/M_{GMNIA} value of 0.89 occurs in member C24, which has a M_{DC}/M_{pl} value of
593 0.24. These two members correspond to the least heavily loaded members in bending and therefore the
594 accuracy of the moment predictions is deemed reasonable.

595 For all design cases, C21 is the critical member that governs failure. For DC1, DC3, DC4 and DC5 the
596 bending moments in this critical member are well predicted with M_{DC}/M_{GMNIA} values of 0.96, 1.00, 1.05
597 and 1.04, respectively. As observed in Kucukler, Gardner & Macorini (2016), DC2 does not consider
598 the influence of the differential rates of plasticity in the structure on the distribution of internal forces
599 and moments and therefore results in the least accurate predictions of ultimate load and distribution of
600 forces/moments when compared with the benchmark results. The additional notional load (H_{ANL}), used
601 in DC2 to mimic the influence of plasticity and residual stresses accounted for in τ_b, impacts the
602 behavior of the full frame, rather than just the highly loaded members, and overestimates the maximum
603 bending moment resisted by the critical member (C21) by 26% in comparison to GMNIA.

604 **Asymmetric Frame**

605 In this sub-section, the second order elastic (GNA/GNIA) and inelastic (GMNIA) design methods
606 presented herein are applied to the multistory asymmetric frame shown in Fig. 12, with ferritic stainless
607 steel material properties (E = 200000 N/mm^2, F_y = 205 N/mm^2, F_u = 415 N/mm^2, n = 14). The
608 benchmark results were obtained by means of geometrically and materially nonlinear analysis with
609 imperfections (L/1000 + residual stresses) using shell finite elements.

610 The ultimate load factors of the frame α_{DC}, calculated as the load level for which the utilisation rate of
611 the critical member becomes equal to unity, for the different design cases (DC1-5), as well as the
612 ultimate load factor obtained from the benchmark shell FE model are presented in Table 11 and shown
613 in Fig. 13. The α_{DC} values were determined through iteration for Design Cases 1, 3 and 4, with the
614 stiffness reduction factors recalculated considering the first order member forces at the load factor α_{DC}.
615 However, note that in the considered frame, the axial loads in the members were all less than P/P_{ns} =
616 0.2 and consequently τ_b = 1.0 in all cases (see Fig. 4c); this explains the similar design predictions for
617 the four elastic design options (DC1-4). The capacity predictions for all design cases are safe sided. The

618 behavior of the frame is best represented in DC5 since all material and geometric nonlinearities are
619 explicitly modeled, leading to the most accurate prediction of both the distribution of internal forces
620 and moments and structural capacity.

621 **SUMMARY OF DESIGN PROPOSALS AND WORKED EXAMPLES**

622 For the design of stainless steel members and structures by second order elastic analysis (GNA/GNIA),
623 the stiffnesses (flexural, axial, torsional) of all members must be uniformly reduced by the general
624 stiffness reduction factor τ_g (equal to 0.7 in AISC 370 and 0.9 in ASCE-8), as given in Table 2, and the
625 flexural stiffness of the members contributing to the stability of the structure must be reduced by a
626 further stiffness reduction factor τ_b, as given by Eq. (8). Alternatively to the use of τ_b, an additional
627 notional load (H_{ANL}) of 0.002 of the total factored gravity load applied at each story may be imposed.
628 In all cases, a notional load (H_{NL}) equal to 0.002 of the total factored gravity load acting at each story
629 to represent the effects of frame out-of-plumbness must be imposed. Buckling checks should be
630 performed to verify the stability of individual members, unless member imperfections are modeled, in
631 which case, only cross-section checks are required. The cross-section checks may be conducted using
632 the CSM, with $\Lambda = 5$ for this application of the method.

633 For the design of stainless steel members and structures by second order inelastic analysis (GMNIA)
634 with strain limits, the influence of the material nonlinearity on the structural response is directly
635 modeled through the definition of the full stress-strain curve of the material. Initial geometric
636 imperfections and residual stresses may be either individually modeled or their combined effect may be
637 considered through the use of equivalent geometric imperfections. Cross-section failure may be defined
638 in beam finite element models through the application of the CSM strain limits, as given by Eqs. (30)
639 and (31). To allow for the beneficial influence of moment gradients, the maximum compressive strains
640 output from the second order inelastic analysis (GMNIA) at each cross-section may be averaged over
641 the elastic local buckling half-wavelength L_{el}. Failure of a system is defined either at the load level at
642 which the CSM strain limit is reached, or, in stability dominated cases, at the load level at which the
643 analysis reaches a peak, whichever occurs first.

644 Two worked examples are presented in this section to illustrate the application of the proposed approach
645 of design by second order elastic analysis (GNA/GNIA) with stiffness reduction for stainless steel
646 structures. Worked Example 1 considers an austenitic stainless steel W6×16 beam-column subjected

to combined compression and major axis bending, as shown in Fig. 14, while Worked Example 2 considers a two-story duplex stainless steel portal frame, as shown in Fig. 15.

Worked Example 1

Worked Example 1 considers, using Design Case 1, a laterally-restrained austenitic grade 304 stainless steel (F_y = 205 N/mm^2, F_u = 515 N/mm^2, E = 193000 N/mm^2) W6×16 member with a length L = 3810 mm subjected to a major axis bending moment M_a = 20.6 kNm and an axial compression N_a = 141.3 kN, as shown in Fig. 14. The material and geometric properties are included in Fig. 14. Considering the width-to-thickness ratios of the cross-section elements, both the flange and web are compact when the cross-section is under flexure ($b/t \leq 0.41\sqrt{E/F_y}$ and $h/t_w \leq 2.54\sqrt{E/F_y}$) and nonslender under axial compression ($b/t \leq 0.41\sqrt{E/F_y}$ and $h/t_w \leq 1.24\sqrt{E/F_y}$). It is first necessary to calculate the stiffness reduction factors under the applied loading. Next, a second order elastic analysis (GNA) of the member with reduced stiffness is performed and the maximum force and moment in the member is extracted at the applied load level. The capacity of the member is then verified using the member buckling check.

Stiffness reduction factors

The material properties for grade 304 stainless steel were taken as F_y = 205 N/mm^2, E = 193000 N/mm^2 and n = 7. Since the member is subjected to major axis buckling, the corresponding effective strain hardening exponent $n_{eff} = 0.55n = 3.85$ is used. For the applied axial load, the stiffness reduction factor τ_b is calculated as:

$$\tau_b = \frac{1}{1 + 0.002 n_{eff} \frac{E}{F_y} \left(\frac{P}{P_y}\right)^{n_{eff}-1}}$$

$$\tau_b = \frac{1}{1 + 0.002(3.85) \frac{193000}{205} \left(\frac{141.3}{619.8}\right)^{3.85-1}} = 0.903$$

Combined with the general stiffness reduction factor τ_g = 0.7, the stiffness of the member must be reduced by $\tau_g \tau_b$ = 0.632.

Beam FE analysis – second order elastic analysis

The member length L of 3810 mm was discretised into 30 elements and a second order elastic analysis (GNA) with stiffness reduction was carried out. Note that a smaller number of elements can be used

672 when justified through a mesh convergence study. Fig. 14b shows the resulting bending moment
673 diagram at the applied load level. From the analysis, the required compressive and flexural strengths P_r
674 = 141.3 kN and M_{rx} = 24.4 kNm, respectively, were determined.

675 *Determine available compressive strength*

676 The nominal compressive strength P_n must be determined based on the limit state of flexural buckling.
677 The member considered has a slenderness ratio L/r = 3810/66.12 = 57.6. Since $L/r > 0.891\sqrt{E/F_y}$
678 and $L/r \leq 5.62\sqrt{E/F_y}$, the critical stress F_{cr} is given by:

679 $$F_{cr} = 1.2\left(\beta_1^{\left(\left(\frac{F_y}{F_e}\right)^{\alpha}\right)}\right)F_y = 1.2\left(0.455^{\left(\left(\frac{205}{574}\right)^{0.58}\right)}\right)205 = 159\ \mathrm{N/mm^2}$$

680 Therefore, the nominal compressive strength $P_n = AF_{cr}$ = 482.1 kN and the available compressive
681 strength P_c is $\phi_c P_n$ = 433.9 kN (LRFD).

682 *Determine available flexural strength*

683 For a member bending about the major axis, the limit states of yielding and lateral-torsional buckling
684 apply. However, the considered member has adequate restraint to prevent lateral-torsional buckling and
685 consequently the limit state of yielding will control. Since the cross-section has compact web and
686 flanges, the nominal flexural strength is:

687 $$M_{nx} = F_y Z_x = 38.7\ \mathrm{kNm}$$

688 Therefore, the available flexural strength M_{cx} is $\phi_c M_{nx}$ = 34.9 kNm (LRFD).

689 *Resistance check*

690 Since $P_r/P_c \geq 0.2$, the resistance is assessed using the interaction equation:

691 $$\frac{P_r}{P_c} + \frac{8}{9}\frac{M_{rx}}{M_{cx}} \leq 1.0$$

692 And

693 $$\frac{141.3}{433.9} + \frac{8}{9}\frac{24.4}{34.9} = 0.95$$

694 Therefore, the chosen W6×16 section is adequate.

Note that a similar process is applied for the design of cold-formed members using ASCE-8, but with the following changes: (1) the effective strain hardening value n_{eff} = 0.45n and τ_g = 0.9, (2) the compressive strength would be calculated according to Section 5 of ASCE-8 (incorporating a degree of strain hardening) and (3) the ASCE-8 moment-axial interaction equation i.e. Eq. (19) would be employed.

Worked Example 2

Worked Example 2 considers, using Design Case 3, a two story duplex grade S32101 stainless steel (F_y = 450 N/mm^2, F_u = 650 N/mm^2, E = 200000 N/mm^2) frame, restrained out-of-plane, as shown in Fig. 15. The material and geometric properties assumed are included in Fig. 15. Member imperfections are modeled with an amplitude of L/1000, and out-of-plumbness is considered through the application of notional loads (H_{NL}) equal to 0.002 times the gravity load at each story. Considering the width-to-thickness ratios of the HEB 340 cross-section, both the flange and web elements are compact when the cross-section is under flexure ($b/t_f \leq 0.41\sqrt{E/F_y}$ and $h/t_w \leq 2.54\sqrt{E/F_y}$) and nonslender under axial compression ($b/t_f \leq 0.41\sqrt{E/F_y}$ and $h/t_w \leq 1.24\sqrt{E/F_y}$). The proposed stiffness reduction method is implemented through the following key steps:

(1) Perform a linear elastic analysis (LA) considering out-of-plumbness.
(2) Calculate the stiffness reduction factors τ_b using Eq. (8) based on the member forces determined through the LA for each column in the system.
(3) Reduce the Young's modulus E and shear modulus G of all members by τ_g as well as the flexural stiffnesses (i.e. the moments of inertia (second moments of area) about the principal axes) of the columns by τ_b.
(4) Perform a geometrically nonlinear analysis (GNIA) considering out-of-plumbness and member imperfections.
(5) Since member imperfections are modeled, carry out cross-section checks using the internal member forces obtained from the GNIA. Assess the adequacy of the structure.

Beam FE analysis – first order elastic analysis

All members were discretised into 30 elements and a first order elastic analysis of the frame was carried out. The section forces (SF_i, where i is the column label) in the columns are extracted as:

SF_{C1} = 1648.8 kN, SF_{C2} = 1950.4 kN, SF_{C3} = 842.3 kN, SF_{C4} = 957.1 kN

Stiffness reduction factors

The material properties for grade S32101 stainless steel were taken as F_y = 450 N/mm^2, E = 200000 N/mm^2 and n = 8. Since the members are buckling about the major axis, the corresponding effective strain hardening exponent n_{eff} = 0.55n = 4.4 is used. For the applied axial load, the stiffness reduction factor τ_b is calculated for each column as

$$\tau_b = \frac{1}{1 + 0.002 n_{eff} \frac{E}{F_y} \left(\frac{P}{P_y}\right)^{n_{eff}-1}}$$

The stiffness reduction factors, calculated for each member of the frame, are given in Table 12.

Beam FE analysis – second order elastic analysis

The members were discretised into 30 elements, and now a second order elastic analysis (GNIA) with stiffness reduction is carried out. From the analysis, the required compressive and flexural strengths, P_r and M_r, respectively, at the critical cross-section of each member is determined, as listed in Table 13.

Determine available compressive strength

Since member imperfections are modeled in the analysis, the nominal compressive strength of the members P_n is taken as the cross-section compressive strength F_yA. Therefore, the nominal compressive strength P_n is equal to 7408.8 kN and the available compressive strength P_c is $\phi_c P_n$ = 6667.9 kN (LRFD).

Determine available flexural strength

For major axis flexure, the limit states of yielding and lateral-torsional buckling apply. However, the member has adequate restraint to prevent lateral-torsional buckling and consequently the limit state of yielding will control. Since the cross-section has compact web and flanges, the nominal flexural strength is:

$$M_{nx} = F_y Z_x = 1043.5 \text{ kNm}$$

Therefore, the available flexural strength M_{cx} is $\phi_c M_{nx}$ = 939.2 kNm (LRFD).

Resistance check

747 For members C1 and C2, $P_r/P_c \geq 0.2$ and the resistance is assessed using the following interaction
748 equation:

749 $$\frac{P_r}{P_c} + \frac{8}{9}\frac{M_{rx}}{M_{cx}} \leq 1.0$$

750 For members C3, C4, B1 and B2, $P_r/P_c < 0.2$ and the resistance is assessed using the following
751 interaction equation:

752 $$\frac{P_r}{2P_c} + \frac{M_{rx}}{M_{cx}} \leq 1.0$$

753 The results of the cross-section checks on the six frame members are presented in Table 14. For all
754 members, the interaction equation is less than unity; therefore, the frame is adequate.

755 Note that for structures composed of cold-formed members and designed using ASCE-8, the following
756 changes would need to be made: (1) the effective strain hardening value $n_{eff} = 0.45n$ and $\tau_g = 0.9$, (2) the
757 compressive strength would be calculated according to Section 5 of ASCE-8 (incorporating a degree of
758 strain hardening) and (3) the ASCE-8 moment-axial interaction equation i.e. Eq. (15) would be
759 employed.

760 **CONCLUSIONS**

761 Stability design rules for stainless steel structures have been established in this paper. For design by
762 second order elastic analysis (also referred to as geometrically nonlinear analysis (GNA) with
763 imperfections (GNIA)), two stiffness reductions factors are defined: (1) a general stiffness reduction
764 factor τ_g, to be applied to all member stiffnesses (axial, flexural, torsional) to account for the
765 development and spread of plasticity and (2) τ_b, to account for the additional reduction in the flexural
766 stiffness of compression members under increasing axial load due to the effects of yielding and residual
767 stresses. The influence of the varying degree of roundedness of the stress-strain behavior on the level
768 of stiffness reduction for the different grades of stainless steel is reflected in the strain hardening
769 exponent n that features in the Ramberg-Osgood formulation. A value of $\tau_g = 0.7$ for AISC 370 and τ_g
770 $= 0.9$ for ASCE-8 is proposed; the different values for the two specifications reflect the different
771 buckling curves and axial-bending interaction expressions and end-points employed.

772 Shell finite element models of the stainless steel members and frames have been developed, validated
773 against experimental results from the literature, and employed to verify the proposed design rules for a
774 wide range of cases. The proposed stiffness reduction factors τ_b and τ_g result in safe sided average

capacity predictions compared with the benchmark shell FE results. The level of scatter in the predictions is similar to that of the carbon steel rules of AISC 360. Comparisons have also been made against the new provisions in AISC 370 for design by second order inelastic analysis (also referred to as geometrically and materially nonlinear analysis with imperfections (GMNIA)) with strain limits; this represents the most accurate design approach. The reliability of the design proposals has been demonstrated through statistical analyses, where it was shown that a resistance factor ϕ of 0.9 can be safely adopted.

The design provisions presented herein are due to be incorporated into the new upcoming AISC 370 Specification for hot-rolled and welded stainless steel structures and the revised ASCE-8 Specification for the design of cold-formed stainless steel structures.

ACKNOWLEDGEMENTS

Funding for this investigation was received from the Engineering and Physical Sciences Research Council (EPSRC) through the EPSRC Doctoral Prize scheme.

DATA AVAILABILITY STATEMENT

Some or all data, models, or code that support the findings of this study are available from the corresponding author upon reasonable request.

REFERENCES

ABAQUS (2014) *Abaqus CAE User's Manual, Version 6.14*. Pawtucket, USA, Hibbitt, Karlsson & Sorensen, Inc.

Afshan, S., Francis, P., Baddoo, N.R. & Gardner, L. (2015) Reliability analysis of structural stainless steel design provisions. *Journal of Constructional Steel Research*. 114, 293–304.

Afshan, S. & Gardner, L. (2013) The continuous strength method for structural stainless steel design. *Thin-Walled Structures*. 68, 42–49.

AISC (2016a) *AISC 303-16 Code of standard practice for steel buildings and bridges*. AISC.

AISC (2016b) *AISC 360. Specification for Structural Steel Buildings*. AISC.

AISC (2021) *AISC 370. Specification for Structural Stainless Steel Buildings. Draft for public review.* AISC.

AISI (2016) *AISI S100-16. North American Specification for the Design of Cold-Formed Steel Structural Members*. AISI.

Arrayago, I., Real, E. & Gardner, L. (2015) Description of stress-strain curves for stainless steel alloys. *Materials and Design*. 87, 540–552.

ASCE (2021) *ASCE-8-21: Specification for the Design of Cold-Formed Stainless Steel Structural Members. Draft for public review.* ASCE.

Baddoo, N.R. & Francis, P. (2014) Development of design rules in the AISC Design Guide for structural stainless steel. *Thin-Walled Structures*. 83, 200–208.

Baddoo, N.R., Meza, F.J. & Gardner, L. (2020) *Proposed overstrength for AISC 370 and ASCE 8.* SCI Report.

812 Bartlett, F.M., Dexter, R.J., Graeser, M.D., Jelinek, J.J., et al. (2003) Updating standard shape
813 material properties database for design and reliability. *Engineering Journal, AISC*. 40, 2–14.
814 Bock, M., Gardner, L. & Real, E. (2015) Material and local buckling response of ferritic stainless
815 steel sections. *Thin-Walled Structures*. 89, 131–141.
816 Bu, Y. & Gardner, L. (2019a) Finite element modelling and design of welded stainless steel I-section
817 columns. *Journal of Constructional Steel Research*. 152, 57–67.
818 Bu, Y. & Gardner, L. (2019b) Laser-welded stainless steel I-section beam-columns: Testing,
819 simulation and design. *Engineering Structures*. 179, 23–36.
820 Chan, S.L., Liu, Y.P. & Liu, S.W. (2011) Structural design in the post-effective length era. *Procedia*
821 *Engineering*. 14, 1005–1012.
822 Deierlein, G. (2003) Background and Illustrative Examples on Proposed Direct Analysis Method for
823 Stability Design of Moment Frames. *Report on behalf of AISC TC 10*. 1–17.
824 Ellobody, E. & Young, B. (2005) Structural performance of cold-formed high strength stainless steel
825 columns. *Journal of Constructional Steel Research*. 61, 1631–1649.
826 EN 1993-1-4:2006 + A1: (2015) *Eurocode 3 - Design of steel structures - Part 1-4: General rules -*
827 *Supplementary rules for stainless steels*. Brussels, CEN.
828 EN 1993-1-5 (2009) *Eurocode 3 - Design of steel structures - Part 1-5 : Plated structural elements*.
829 Brussels, CEN.
830 Fieber, A., Gardner, L. & Macorini, L. (2019a) Design of structural steel members by advanced
831 inelastic analysis with strain limits. *Engineering Structures*. 199, 109624.
832 Fieber, A., Gardner, L. & Macorini, L. (2019b) Formulae for determining elastic local buckling half-
833 wavelengths of structural steel cross-sections. *Journal of Constructional Steel Research*. 159,
834 493–506.
835 Fieber, A., Gardner, L. & Macorini, L. (2020) Structural steel design using second-order inelastic
836 analysis with strain limits. *Journal of Constructional Steel Research*. 168, 105980.
837 Gardner, L. (2008) The continuous strength method. *Proceedings of the Institution of Civil Engineers*
838 *- Structures and Buildings*. 161 (3), 127–133.
839 Gardner, L. & Nethercot, D.A. (2004) Numerical modeling of stainless steel structural components —
840 A consistent approach. *Journal of Structural Engineering ASCE*. 130 (10), 1586–1601.
841 Gardner, L., Wang, F. & Liew, A. (2011) Influence of strain hardening on the behavior and design of
842 steel structures. *International Journal of Structural Stability and Dynamics*. 11 (5), 855–875.
843 Jandera, M., Gardner, L. & Machacek, J. (2008) Residual stresses in cold-rolled stainless steel hollow
844 sections. *Journal of Constructional Steel Research*. 64 (11), 1255–1263.
845 Kucukler, M. & Gardner, L. (2018) Design of laterally restrained web-tapered steel structures through
846 a stiffness reduction method. *Journal of Constructional Steel Research*. 141, 63–76.
847 Kucukler, M. & Gardner, L. (2019) Design of web-tapered steel beams against lateral-torsional
848 buckling through a stiffness reduction method. *Engineering Structures*. 190, 246–261.
849 Kucukler, M., Gardner, L. & Macorini, L. (2014) A stiffness reduction method for the in-plane design
850 of structural steel elements. *Engineering Structures*. 73, 72–84.
851 Kucukler, M., Gardner, L. & Macorini, L. (2016) Development and assessment of a practical stiffness
852 reduction method for the in-plane design of steel frames. *Journal of Constructional Steel*
853 *Research*. 126, 187–200.
854 Kucukler, M., Gardner, L. & Macorini, L. (2015) Flexural-torsional buckling assessment of steel
855 beam-columns through a stiffness reduction method. *Engineering Structures*. 101, 662–676.
856 Kucukler, M., Xing, Z. & Gardner, L. (2020) Behaviour and design of stainless steel I-section
857 columns in fire. *Journal of Constructional Steel Research*. 164, 105890.
858 Liew, J.Y.R. (1992) *Advanced analysis for frame design*. Purdue University (PhD Thesis).
859 Liew, J.Y.R., White, D.W. & Chen, W.F. (1994) Second-order refined plastic-hinge analysis for
860 frame design. Part I. *Journal of Structural Engineering ASCE*. 119 (11), 3196–3216.
861 Lin, S.-H., Yu, W.-W. & Galambos, T.V. (1992) ASCE LRFD method for stainless steel structures.
862 *Journal of Structural Engineering ASCE*. 118 (4), 1056–1070.
863 Lui, E.M. & Ge, M. (2005) Analysis and design for stability in the U.S. - An overview. *Steel and*
864 *Composite Structures*. 5 (2), 103–126.
865 Meng, X. & Gardner, L. (2020) Behavior and Design of Normal- and High-Strength Steel SHS and
866 RHS Columns. *Journal of Structural Engineering ASCE*. 146 (11), 04020227.

867 Meza, F.J., Baddoo, N.R. & Gardner, L. (2021) Development of Flexural Buckling Rules for the New
868 AISC Stainless Steel Design Specification. *Proceedings of the 9th European Conference on*
869 *Steel and Composite Structures, Eurosteel 2021*. Sheffield, UK.
870 Mirambell, E. & Real, E. (2000) On the calculation of deflections in structural stainless steel beams:
871 an experimental and numerical investigation. *Journal of Constructional Steel Research*. 54 (1),
872 109–133.
873 Orbison, J.G. (1982) *Nonlinear static analysis of three-dimensional steel frames*. Cornell University
874 (PhD Thesis).
875 prEN 1993-1-4 (2020) Eurocode 3 - Design of steel structures - Part 1-4: General rules -
876 Supplementary rules for stainless steels. *CEN*. Draft 2.
877 SCI (2013) *Steel Design Guide 27: Structural Stainless Steel*. Chicago, AISC.
878 Shen, Y. & Chacón, R. (2020a) Flexural stiffness reduction for stainless steel SHS and RHS members
879 prone to local buckling. *Thin-Walled Structures*. 155, 106939.
880 Shen, Y. & Chacón, R. (2020b) Geometrically non-linear analysis with stiffness reduction for the
881 stability design of stainless steel structures: Application to members and planar frames. *Thin-*
882 *Walled Structures*. 148, 106581.
883 Surovek-Maleck, A.E. (2001) *Second-order inelastic and modified elastic analysis and design*
884 *evaluation of planar steel frames*. Georgia Institute of Technology (PhD Thesis).
885 Surovek-Maleck, A.E. & White, D.W. (2004a) Alternative Approaches for Elastic Analysis and
886 Design of Steel Frames. I: Overview. *Journal of Structural Engineering ASCE*. 130 (8), 1186–
887 1196.
888 Surovek-Maleck, A.E. & White, D.W. (2004b) Alternative approaches for elastic analysis and design
889 of steel frames. II: Verification studies. *Journal of Structural Engineering ASCE*. 130 (8), 1197–
890 1205.
891 Vogel, U. (1985) Calibrating frames. *Stahlbau*. 10 (54), 295–301.
892 Walport, F., Gardner, L. & Nethercot, D.A. (2021) Design of structural stainless steel members by
893 second order inelastic analysis with CSM strain limits. *Thin-Walled Structures*. 159, 107267.
894 Walport, F., Gardner, L. & Nethercot, D.A. (2020) Equivalent bow imperfections for use in design by
895 second order inelastic analysis. *Structures*. 26, 670–685.
896 Walport, F., Gardner, L., Real, E., Arrayago, I., et al. (2019) Effects of material nonlinearity on the
897 global analysis and stability of stainless steel frames. *Journal of Constructional Steel Research*.
898 152, 173–182.
899 Yuan, H.X., Wang, Y.Q., Shi, Y.J. & Gardner, L. (2014) Residual stress distributions in welded
900 stainless steel sections. *Thin-Walled Structures*. 79, 38–51.
901 Yura, J.A. (1971) The effective length of columns in unbraced frames. *AISC Engineering Journal*. 8
902 (2), 37–42.
903 Ziemian, R.D. & Wang, Y. (2019) Design by advanced analysis - 2016 AISC specification. *SDSS*
904 *2019 - International Colloquium on Stability and Ductility of Steel Structures*. Prague, Czech
905 Republic.
906

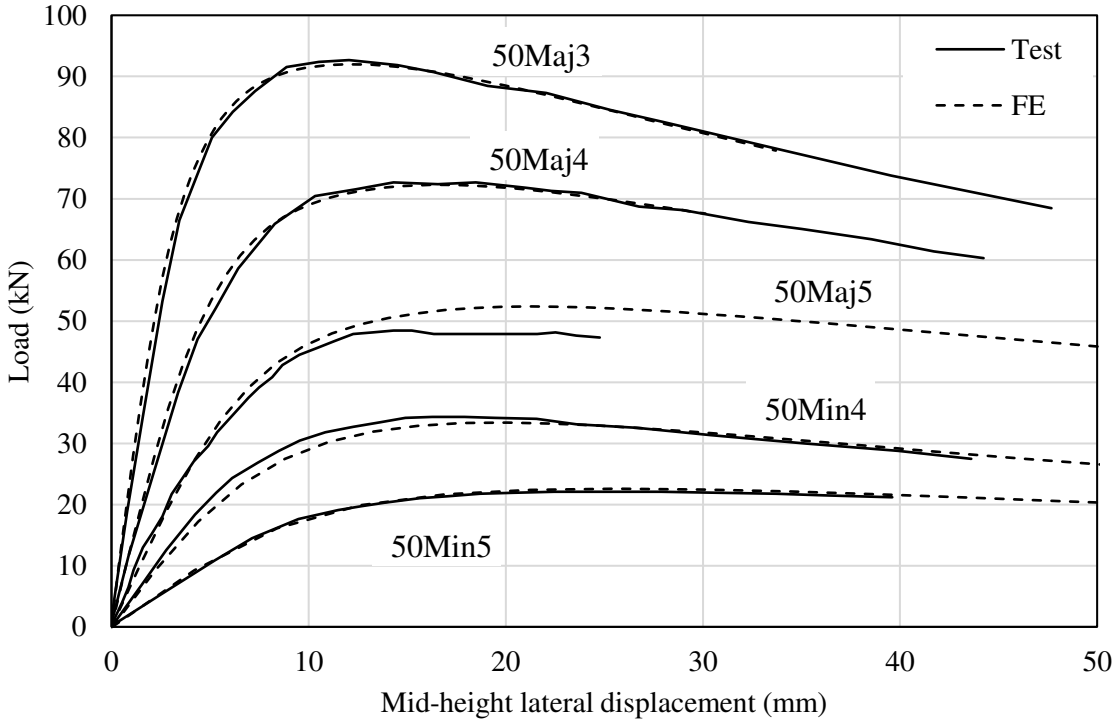

Fig. 1. Shell FE model validation against beam-column tests on an austenitic stainless steel I-50×50×4×4 cross-section reported by Bu and Gardner (2019b).

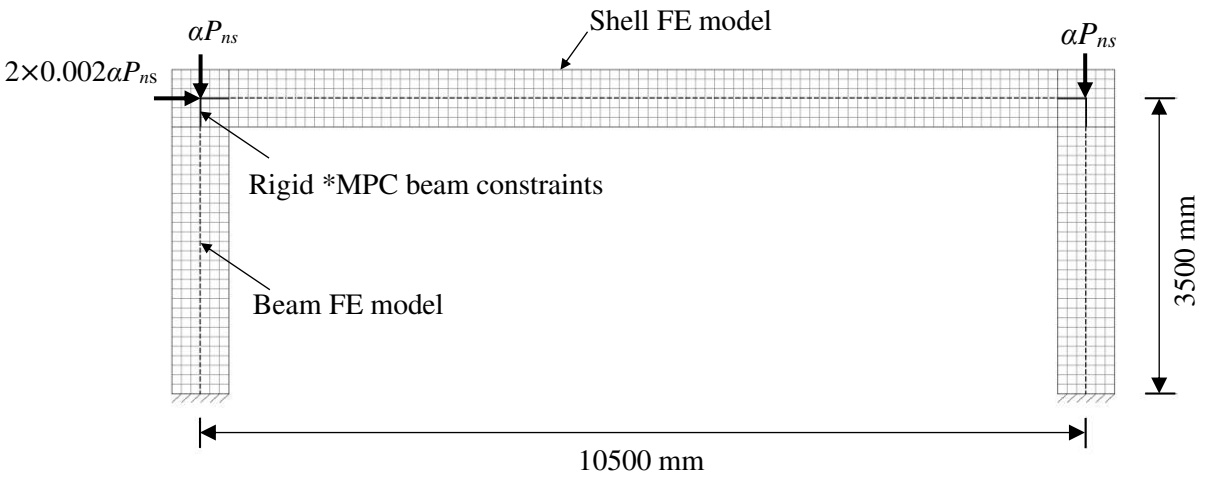

(a) Frame modelling with rigid *MPC beam constraints in beam FE model to represent the rigid beam-to-column connection in the shell FE model

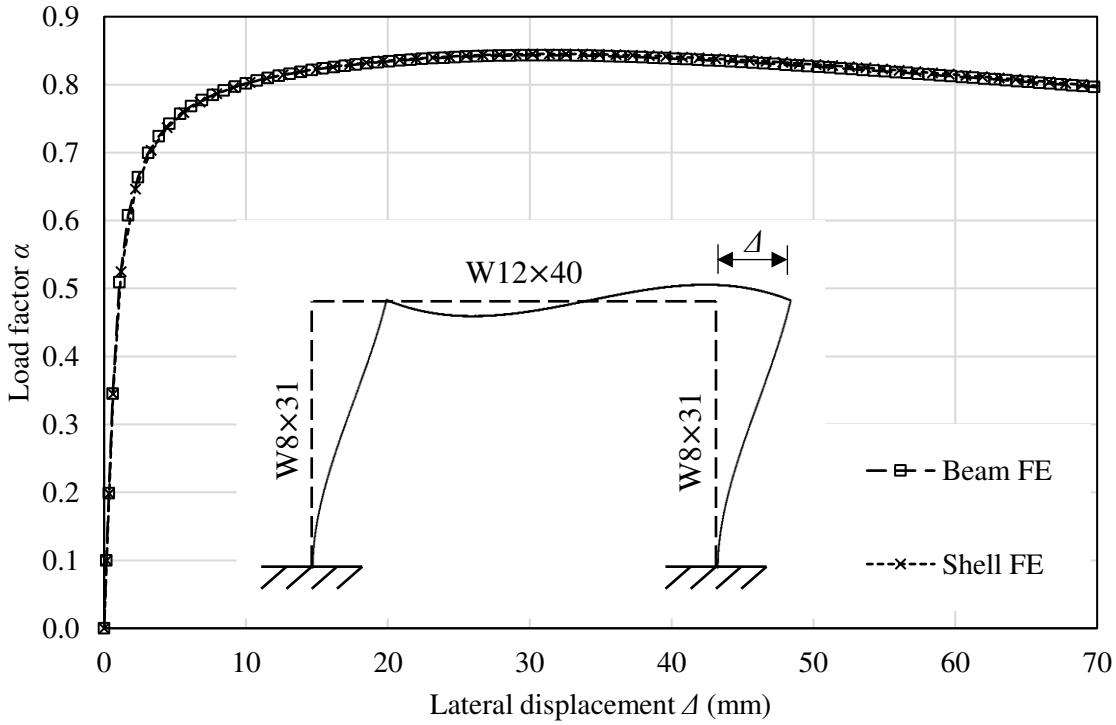

(b) Load-deformation response

Fig. 2. Example austenitic (F_y = 205 N/mm^2, E = 193000 N/mm^2) stainless steel fixed based frame to illustrate the finite element (FE) modeling implemented in this study. Note that in both FE models, the same initial imperfections were included (L/1000 + no residual stresses) to allow for direct comparison.

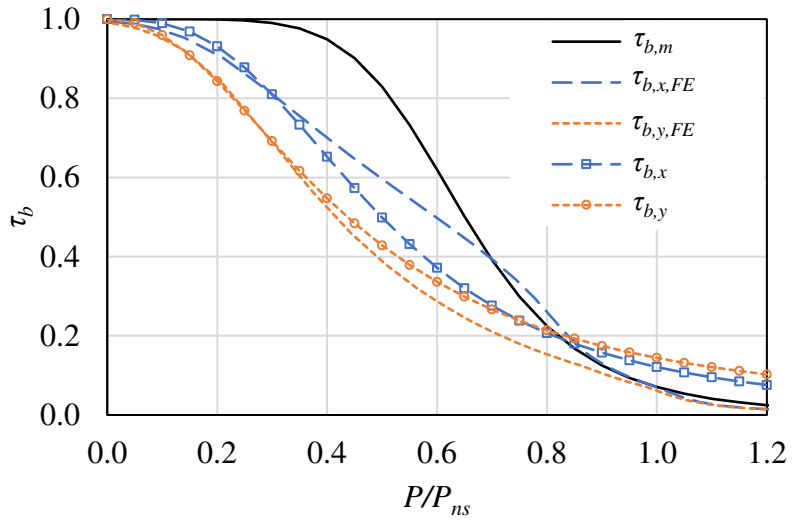

(a) Austenitic stainless steel (F_y = 205 N/mm^2, E = 193000 N/mm^2, n = 7)

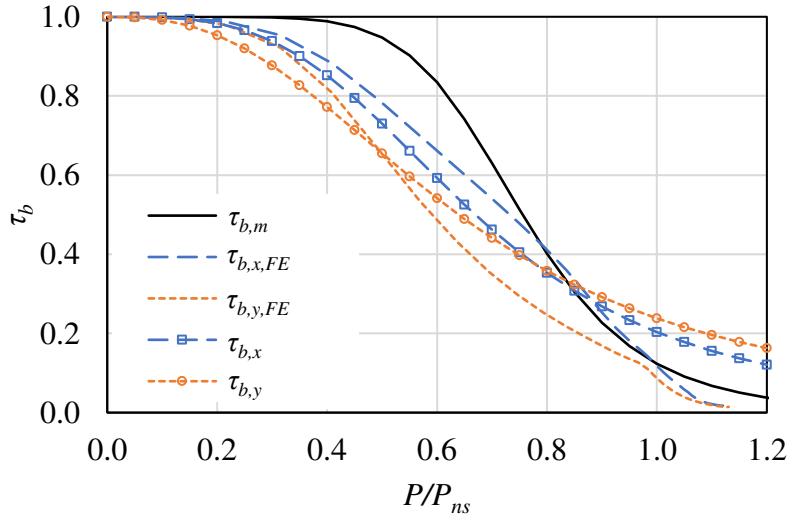

(b) Duplex stainless steel (F_y = 450 N/mm^2, E = 200000 N/mm^2, n = 8)

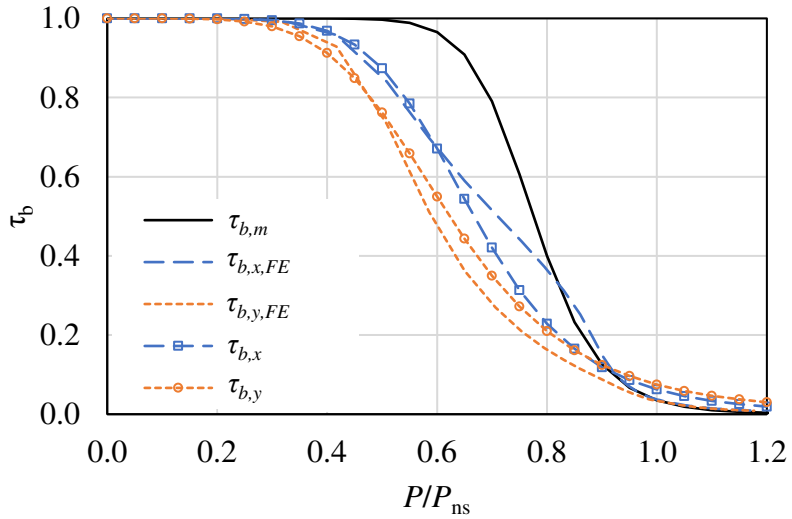

(c) Ferritic stainless steel (F_y = 205 N/mm^2, E = 200000 N/mm^2, n = 14)

Fig. 3. Calibration of effective strain hardening exponents n_{eff} to derive the stiffness reduction factor τ_b to account for the adverse influence of spread of plasticity and residual stresses as a function of the level of axial loading.

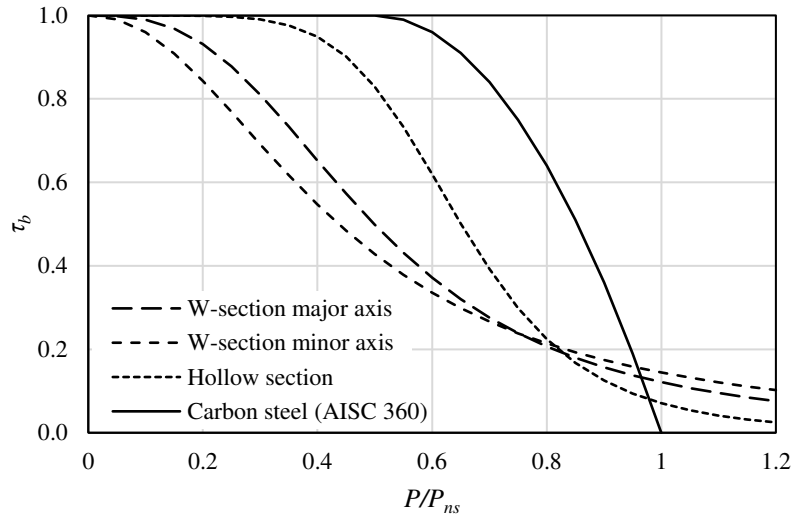

(a) Austenitic stainless steel (F_y = 205 N/mm^2, E = 193000 N/mm^2, n = 7)

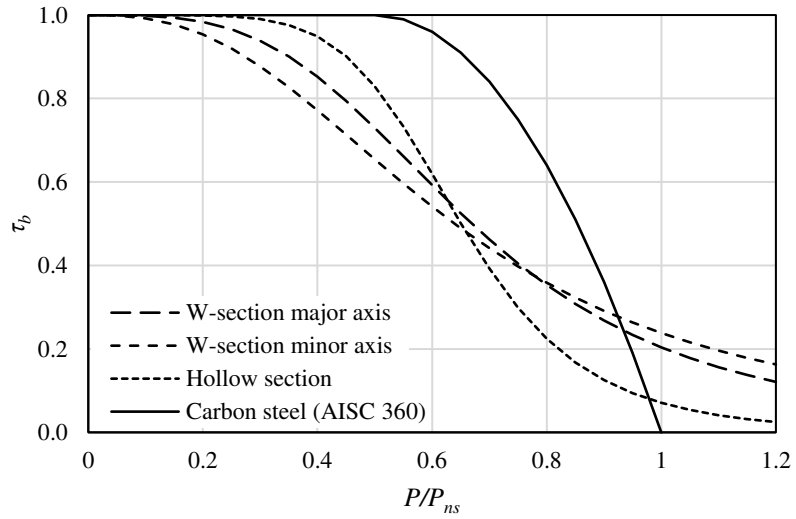

(b) Duplex stainless steel (F_y = 450 N/mm^2, E = 200000 N/mm^2, n = 8)

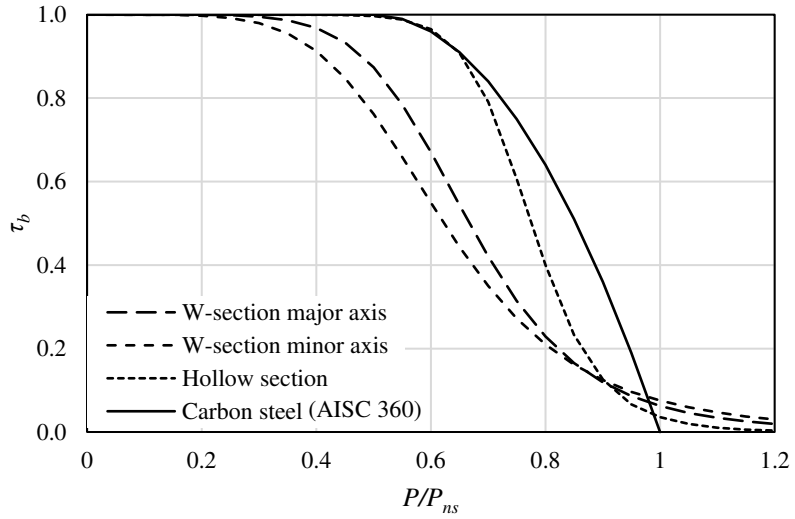

(c) Ferritic stainless steel (F_y = 205 N/mm^2, E = 200000 N/mm^2, n = 14)

Fig. 4. AISC 370 stiffness reduction factor τ_b for typical austenitic, duplex and ferritic grades of stainless steel. For W-section major axis buckling $n_{eff} = 0.55n$, for W-section minor axis buckling $n_{eff} = 0.45n$, and for hollow sections $n_{eff} = n$. In all cases, $n_{eff} \geq 2.5$.

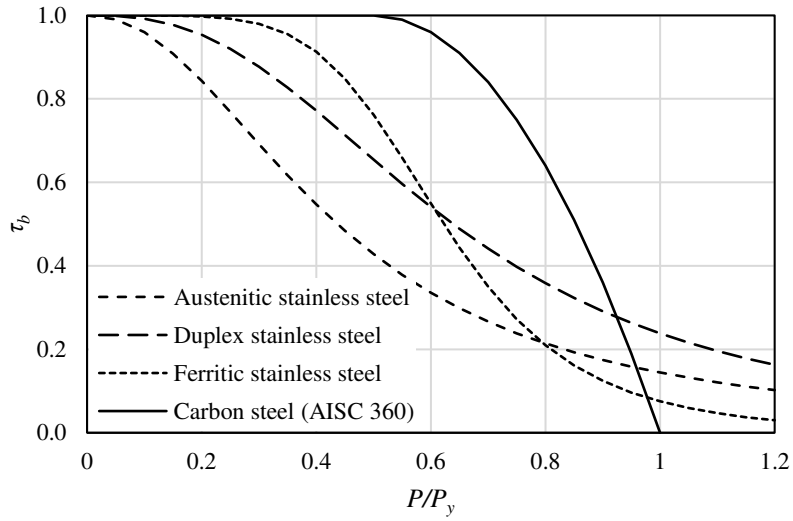

Fig. 5. ASCE-08 stiffness reduction factor τ_b for typical austenitic, duplex and ferritic grades of stainless steel. For all cases $n_{eff} = 0.45n$ (but $n_{eff} \geq 2.5$).

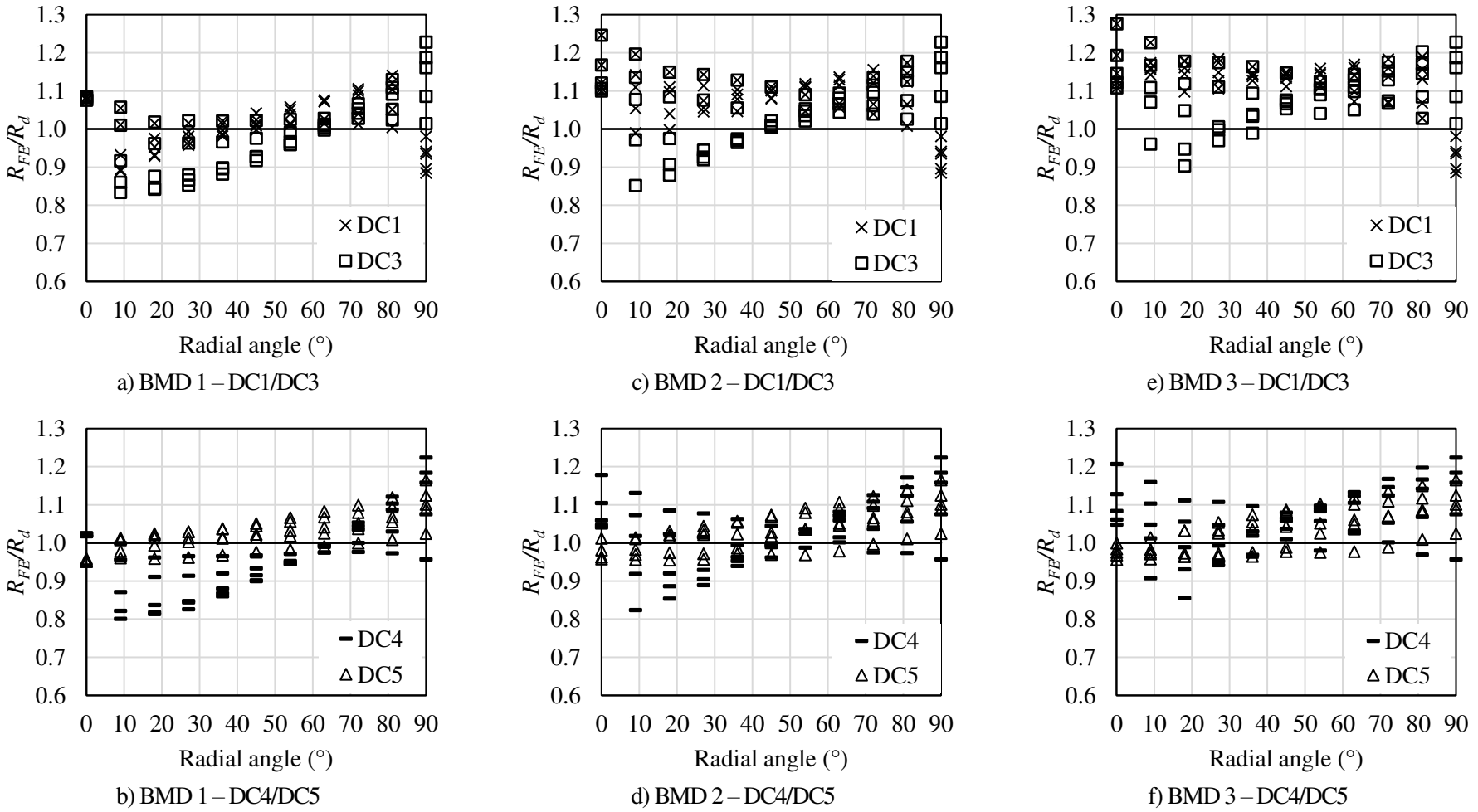

Fig. 6. Comparison of the capacity predictions of austenitic stainless steel W-section columns, beams and beam-columns subjected to major axis bending for the Design Cases (DC) 1 (GNA + τ_g + τ_b + no member imperfections + member check), 3 (GNIA + τ_g + τ_b + member imperfections (L/1000) + cross-section check), 4 (GNIA + τ_g + τ_b + member imperfections (L/1000) + cross-section check + CSM end points) and 5 (GMNIA + member imperfections (equivalent imperfections) + CSM strain limits) against the benchmark shell FE results. Note that a radial angle of 0° corresponds to pure bending while a radial angle of 90° corresponds to pure compression.

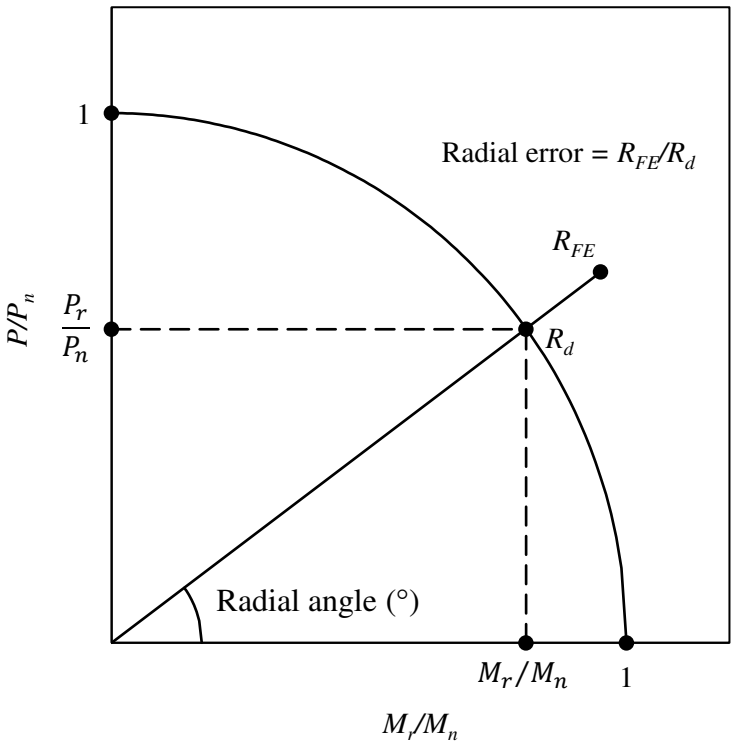

Fig. 7. Definition of radial angle and radial error in normalised *M–P* interaction diagram.

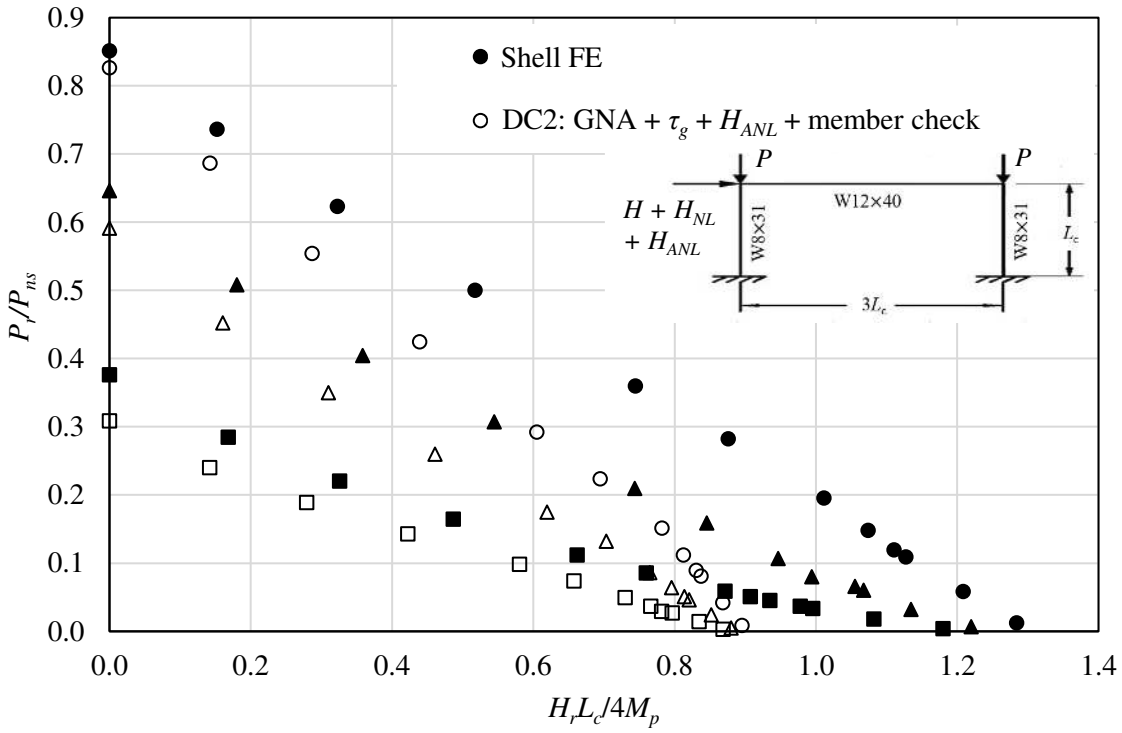

Fig. 8. Comparison of the proposed stiffness reduction method (with τ_g and additional notional loads) against shell benchmark FE results for fixed based austenitic stainless steel portal frames considering three values of column slenderness (L_c = 3.5 m → L/r = 40 (circles); L_c = 6 m → L/r = 68 (triangles); L_c = 10 m → L/r = 113 (squares)). DC2 – GNA + τ_g + H_{ANL}+ no member imperfections + member check.

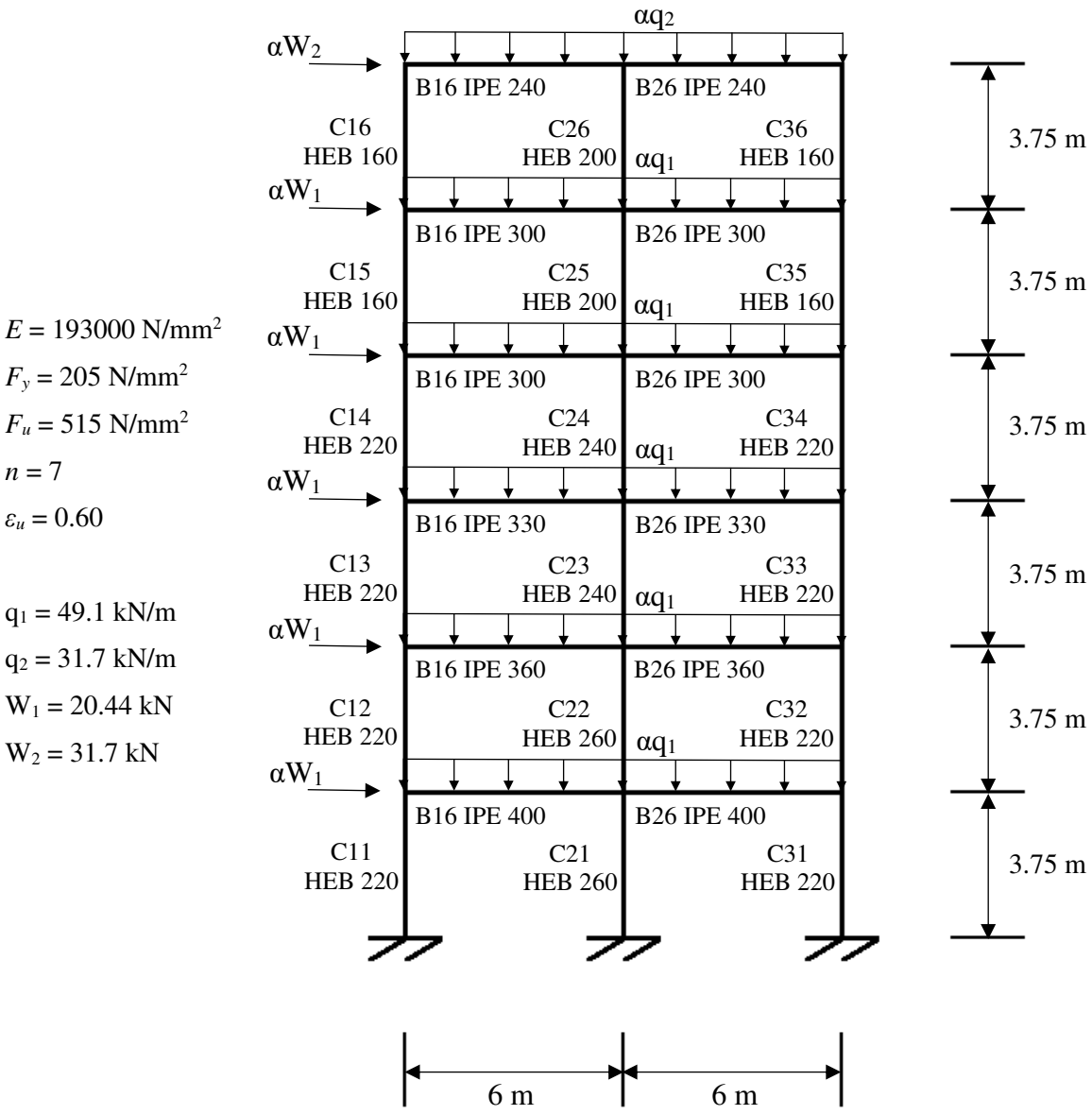

Fig. 9. Geometrical and material properties and loading conditions of the modeled Vogel (1985) frame.

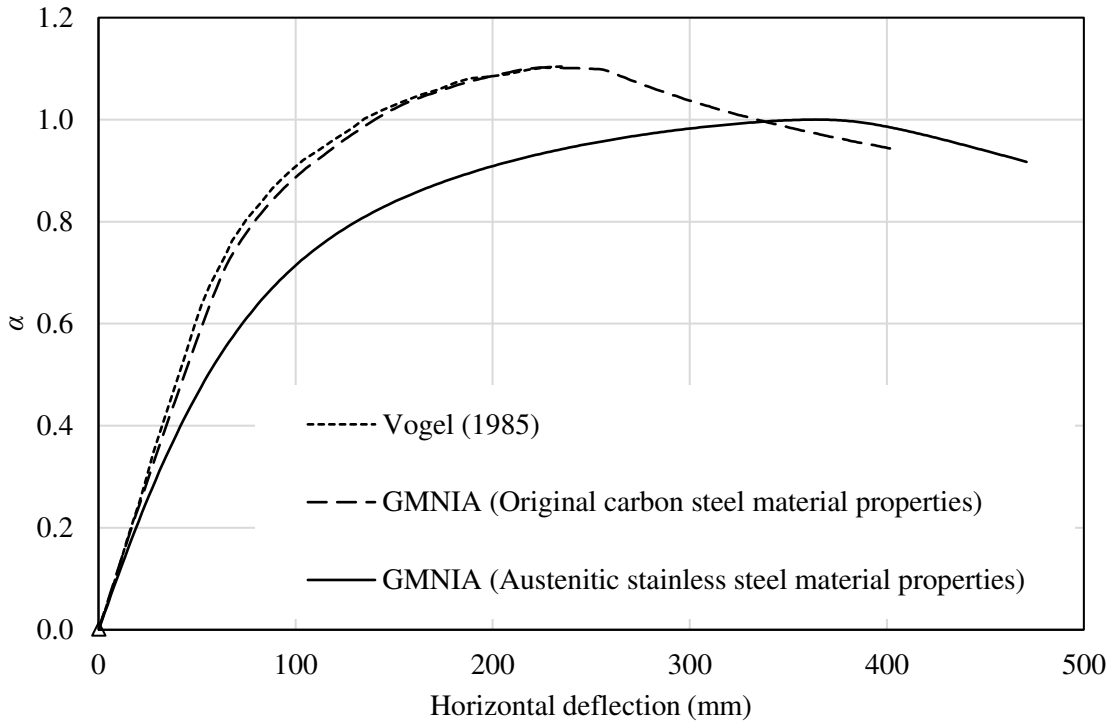

Fig. 10. Load-deflection response of Vogel frame modeled with bilinear carbon steel material stress-strain properties and rounded Ramberg-Osgood (R-O) stainless steel material stress-strain properties.

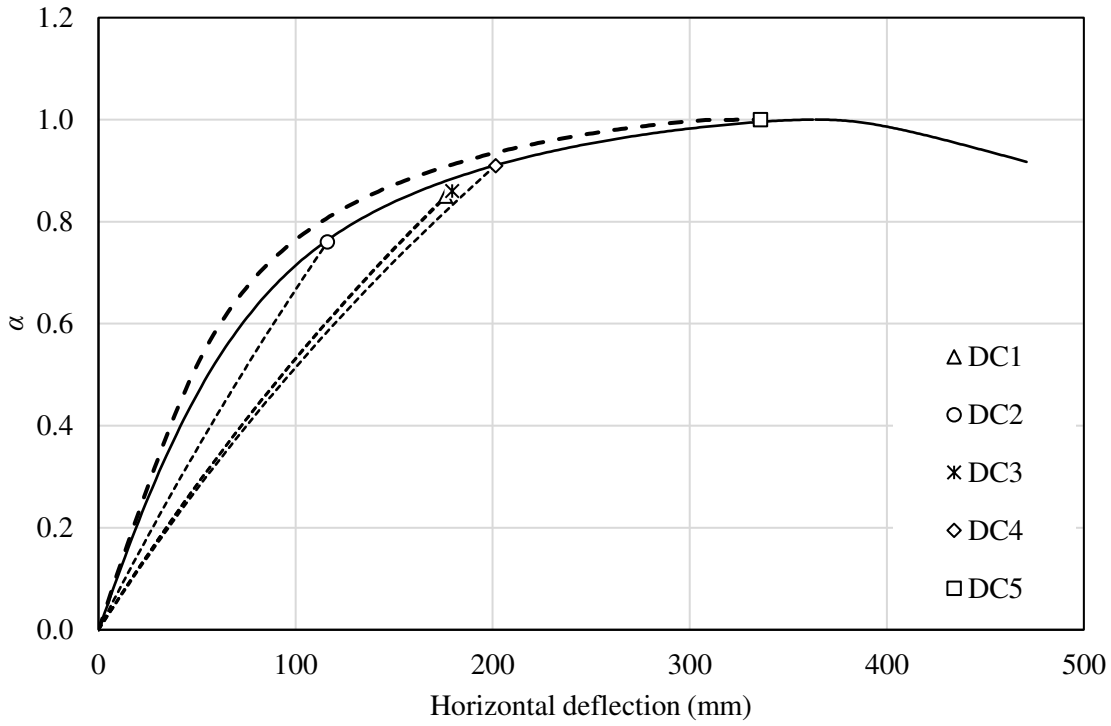

Fig. 11. Benchmark GMNIA load-deflection response of Vogel frame and ultimate load factor predictions for five design cases (DC1-5) considered. DC1: GNA + τ_g + τ_b + no member imperfections + member check, DC2: GNA + τ_g + H_{ANL} + no member imperfections + member check, DC3: GNIA + τ_g + τ_b + member imperfections (L/1000) + cross-section check, DC4: GNIA + τ_g + τ_b + member imperfections (L/1000) + cross-section check with CSM end points, and DC5: GMNIA + member imperfections (equivalent imperfection) + CSM strain limits.

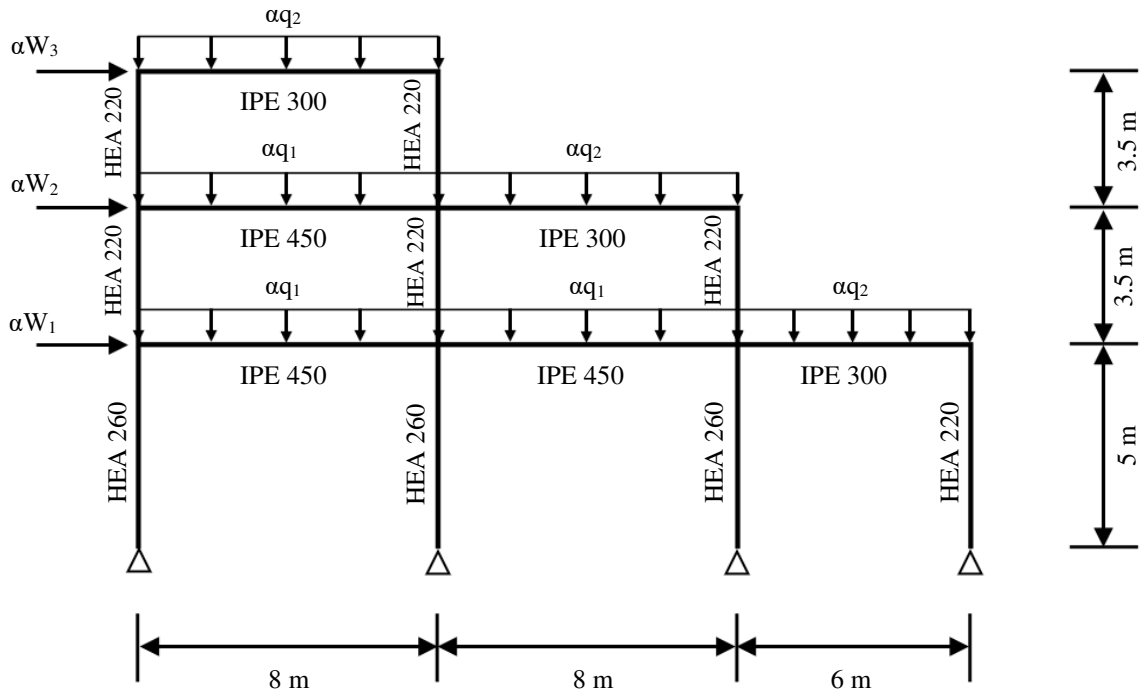

E = 200000 N/mm^2	q_1 = 50 kN/m
F_y = 205 N/mm^2	q_2 = 35 kN/m
F_u = 505 N/mm^2	W_1 = 200 kN
n = 14	W_2 = 180 kN
ε_u = 0.31	W_3 = 35 kN

Fig. 12. Geometrical and material properties and loading conditions of the modeled ferritic stainless steel multistory asymmetric frame.

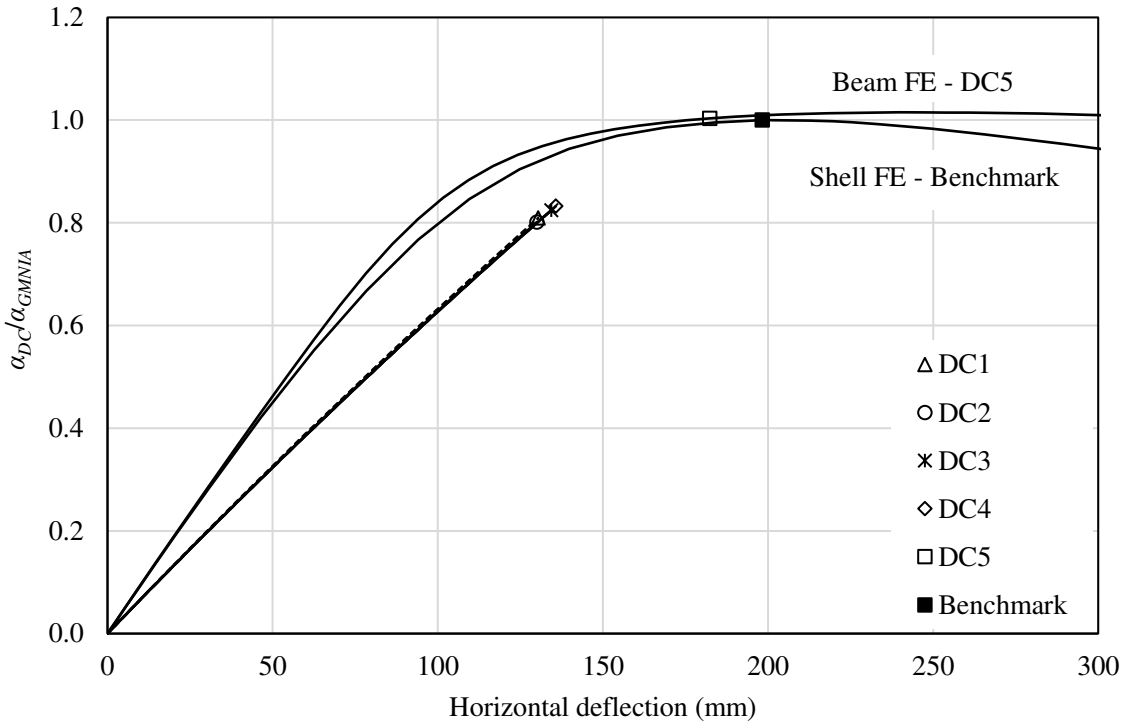

Fig. 13. Ultimate load capacity predictions of the multistory asymmetric frame from the stainless steel design cases (DC1-5) α_{DC} considered normalised by the benchmark capacity α_{GMNIA}. DC1: GNA + τ_g + τ_b + no member imperfections + member check, DC2: GNA + τ_g + H_{ANL} + no member imperfections + member check, DC3: GNIA + τ_g + τ_b + member imperfections (L/1000) + cross-section check, DC4: GNIA + τ_g + τ_b + member imperfections (L/1000) + cross-section check with CSM end points, and DC5: GMNIA + member imperfections (equivalent imperfection) + CSM strain limits.

L = 3810 mm
N_a = 141.3 kN
M_a = 20.6 kNm
n_{eff} = 0.55n

W6×16:

A = 3024 mm^2
I_x = 13219983 mm^4
Z_x = 189019 mm^3

Grade 304

F_y = 205 N/mm^2
F_u = 515 N/mm^2
E = 193000 N/mm^2
n = 7

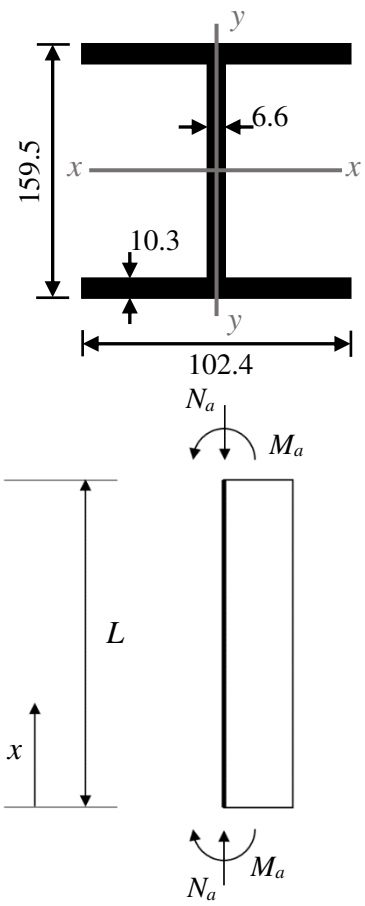

a) Geometric and material properties considered in Worked Example 1

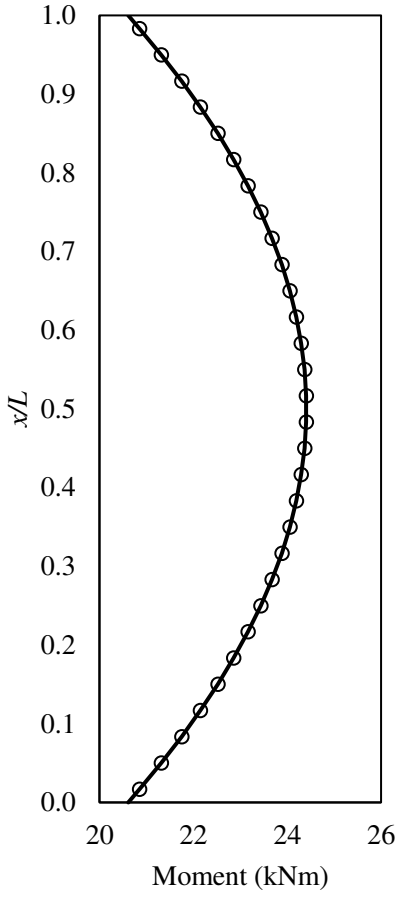

b) Second order bending moments along member at applied loading

Fig. 14. Worked Example 1: W6×16 cross-section under combined compression and major axis bending. All dimensions in mm. Not to scale.

All members
HEB 340:

h = 340 mm
b_f = 300 mm
t_f = 21.5 mm
t_w = 12 mm
A = 16464 mm^2
I_x = 353846248 mm^4
Z_x = 2318952 mm^3

Grade S32101

F_y = 450 N/mm^2
E = 200000 N/mm^2
n = 8
n_{eff} = 0.55n

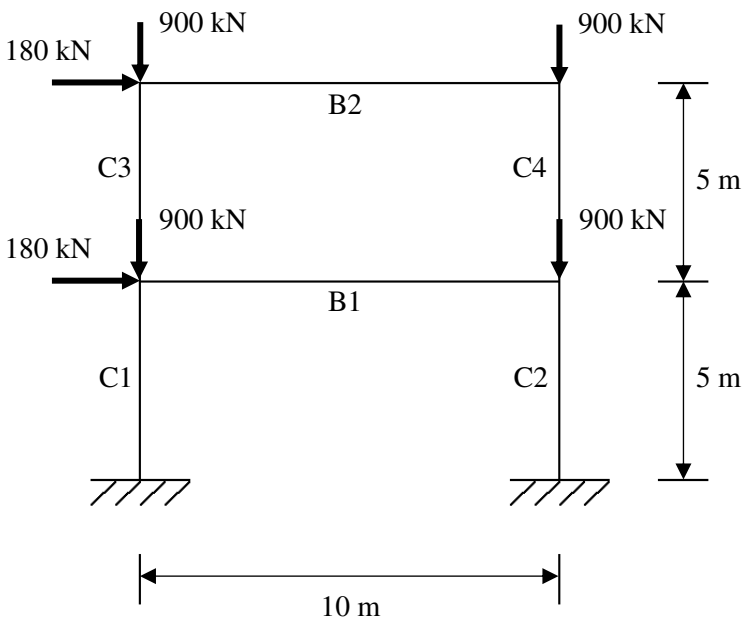

Fig. 15. Worked Example 2: Two-story duplex stainless steel frame.

Table 1. Ramberg-Osgood material model parameters (AISC 2020; ASCE 2020)

Material grade	Young's modulus E (N/mm^2)	Yield (0.2% proof) stress F_y (N/mm^2)	Ultimate stress F_u (N/mm^2)	Ultimate strain ε_u	Strain hardening exponent n	Strain hardening exponent m
Austenitic 304	193000	205	515	0.60	7	2.1
Duplex S32101	200000	450	650	0.31	8	2.9
Ferritic 410S	200000	205	415	0.30	15	2.4

Table 2. Proposed τ function coefficients

Code	Member type	n_{eff} (≥ 2.5)	τ_g	τ_b
AISC 370	Rolled or welded I-shaped sections buckling about the minor axis, and other sections not specified in this table	0.45n	0.7	$\tau_b = \frac{1}{1 + 0.002 n_{eff} \frac{E}{F_y} \left(\frac{P_r}{P_{ns}}\right)^{n_{eff}-1}}$
	Rolled or welded I-shaped sections buckling about the major axis, welded box sections, and round HSS	0.55n		
	Rectangular HSS	n		
ASCE-8	All sections	0.45n	0.9	

Table 3. Design Cases 1 to 5 considered in this study

	Label	Analysis type	Stiffness reduction factors	Notional load coefficient	Capacity check
Design Case 1	DC1	Elastic	$\tau_g + \tau_b$	0.002 (H_{NL} only)	Member check
Design Case 2	DC2	Elastic	τ_g	0.002 + 0.002 ($H_{NL} + H_{ANL}$)	Member check
Design Case 3	DC3	Elastic	$\tau_g + \tau_b$	0.002 (H_{NL} only)	Cross-section check
Design Case 4	DC4	Elastic	$\tau_g + \tau_b$	0.002 (H_{NL} only)	Cross-section check with CSM end points
Design Case 5	DC5	Inelastic	-	0.002 (H_{NL} only)	CSM strain limit

Table 4. AISC 360 flexural buckling coefficients for austenitic, duplex and ferritic stainless steel (Meza, Baddoo & Gardner, 2021)

Member type	α	β_0	β_1	β_2
Rolled or welded I-shaped sections buckling about the minor axis, and other sections not specified in this table	0.56	0.759	0.409	0.69
Rolled or welded I-shaped sections buckling about the major axis, welded box sections, and round HSS	0.58	0.891	0.455	0.82
Rectangular HSS	0.69	1.195	0.501	0.82

Table 5. Imperfection factors α_{eq} for different types of members for calculating the equivalent member imperfection

Member type	Axis of buckling	α_{eq}	
		Austenitic and Duplex	Ferritic
Rectangular HSS	Any	0.49	0.34
Round HSS	Any	0.49	0.34
Rolled or welded I-shaped sections, and welded box sections	Major	0.49	0.49
	Minor	0.76	0.76

Table 6. Summary of comparison between the proposed AISC 370 design approaches and benchmark shell FE results for austenitic (A), duplex (D) and ferritic (F) stainless steel columns, beams and beam-columns considering Design Cases (DC) 1, 2, 3 and 5 – DC1: GNA + τ_g + τ_b + no member imperfections + member check, DC3: GNIA + τ_g + τ_b + member imperfections (L/1000) + cross-section check, DC4: GNIA + τ_g + τ_b + member imperfections (L/1000) + cross-section check with CSM end points, and DC5: GMNIA + member imperfections (equivalent imperfection) + CSM strain limits.

Grade	Cross-section type	Load type	No.	Design by elastic analysis with stiffness reduction									Design by inelastic analysis		
				Design Case 1			Design Case 3			Design Case 4			Design Case 5		
				Radial error R_{FE}/R_{DC1}			Radial error R_{FE}/R_{DC3}			Radial error R_{FE}/R_{DC4}			Radial error R_{FE}/R_{DC5}		
				Ave.	Std.	ϕ	Ave.	Std.	ϕ	Ave.	Std.	ϕ	Ave.	Std.	ϕ
A	W-major	1	55	1.01	0.06	1.08	1.00	0.09	1.04	0.97	0.09	1.00	1.03	0.05	1.09
		2	55	1.08	0.07	1.15	1.06	0.09	1.12	1.03	0.09	1.08	1.03	0.05	1.10
		3	55	1.12	0.07	1.19	1.10	0.07	1.17	1.06	0.08	1.12	1.04	0.06	1.10
		All	165	1.07	0.08	1.13	1.05	0.09	1.10	1.02	0.10	1.06	1.03	0.05	1.10
	W-minor	1	55	1.09	0.12	1.10	1.06	0.15	1.03	1.05	0.14	1.03	1.06	0.03	1.13
		2	55	1.18	0.17	1.14	1.15	0.19	1.08	1.14	0.18	1.07	1.07	0.03	1.14
		3	55	1.24	0.19	1.18	1.20	0.20	1.12	1.19	0.19	1.12	1.07	0.03	1.14
		All	165	1.17	0.18	1.12	1.14	0.19	1.06	1.12	0.18	1.06	1.07	0.03	1.14
	SHS	1	55	1.02	0.09	1.07	1.00	0.11	1.03	0.97	0.10	1.00	1.06	0.06	1.13
		2	55	1.10	0.11	1.13	1.08	0.13	1.08	1.04	0.11	1.06	1.07	0.06	1.14
		3	55	1.15	0.12	1.17	1.12	0.12	1.13	1.08	0.11	1.11	1.08	0.07	1.15
		All	165	1.09	0.12	1.11	1.07	0.13	1.07	1.03	0.12	1.04	1.07	0.07	1.14
D	W-major	1	33	1.02	0.06	0.96	0.98	0.06	0.93	0.99	0.06	0.93	1.01	0.03	0.95
		2	33	1.09	0.06	1.02	1.04	0.06	0.98	1.05	0.06	0.99	1.02	0.04	0.96
		3	33	1.12	0.07	1.05	1.06	0.06	1.00	1.07	0.06	1.01	1.02	0.04	0.96
		All	99	1.08	0.07	1.01	1.03	0.07	0.97	1.04	0.07	0.98	1.02	0.04	0.96
	W-minor	1	33	1.13	0.07	1.06	1.07	0.10	0.98	1.06	0.10	0.97	1.04	0.03	0.98
		2	33	1.22	0.10	1.13	1.15	0.12	1.03	1.14	0.12	1.03	1.04	0.03	0.98
		3	33	1.27	0.13	1.16	1.19	0.13	1.07	1.18	0.12	1.07	1.04	0.04	0.98
		All	99	1.21	0.12	1.10	1.13	0.13	1.01	1.13	0.12	1.01	1.04	0.03	0.98
	SHS	1	33	1.04	0.04	0.98	1.02	0.05	0.96	1.00	0.05	0.94	1.05	0.04	0.99
		2	33	1.11	0.06	1.05	1.08	0.06	1.01	1.05	0.06	0.99	1.06	0.05	1.00
		3	33	1.15	0.07	1.08	1.11	0.06	1.04	1.08	0.05	1.02	1.07	0.05	1.00
		All	99	1.08	0.06	1.01	1.05	0.07	0.99	1.02	0.06	0.96	1.06	0.05	1.00
F	W-major	1	55	1.03	0.06	1.09	0.99	0.07	1.04	0.94	0.08	0.99	1.03	0.05	1.10
		2	55	1.10	0.07	1.17	1.05	0.08	1.11	1.00	0.08	1.06	1.04	0.06	1.11
		3	55	1.14	0.07	1.21	1.08	0.08	1.15	1.03	0.07	1.09	1.04	0.06	1.11

		All	165	1.09	0.08	1.15	1.04	0.09	1.09	0.99	0.09	1.04	1.04	0.06	1.11
	W-minor	1	55	1.11	0.10	1.15	1.05	0.15	1.01	1.02	0.14	1.00	1.09	0.05	1.16
		2	55	1.20	0.15	1.20	1.13	0.20	1.04	1.10	0.18	1.03	1.09	0.05	1.16
		3	55	1.26	0.17	1.24	1.18	0.21	1.08	1.15	0.19	1.07	1.10	0.06	1.17
		All	165	1.19	0.16	1.18	1.12	0.19	1.03	1.09	0.18	1.02	1.09	0.05	1.16
	SHS	1	55	1.05	0.09	1.10	1.03	0.10	1.06	0.98	0.10	1.01	1.07	0.07	1.13
		2	55	1.13	0.11	1.17	1.10	0.12	1.11	1.05	0.11	1.07	1.08	0.07	1.15
		3	55	1.18	0.11	1.22	1.14	0.12	1.16	1.09	0.11	1.12	1.09	0.07	1.15
		All	165	1.12	0.12	1.15	1.09	0.12	1.10	1.04	0.12	1.05	1.08	0.07	1.15

Table 7. Reliability factors considered in this study (Afshan et al. 2015, Baddoo, Meza & Gardner 2020)

	Austenitic stainless steel	Duplex stainless steel	Ferritic stainless steel
M_m	1.25	1.10	1.25
V_m	0.05	0.04	0.05
F_m	0.05	0.05	0.05
V_f	0.19	0.19	0.19

Table 8. Ultimate load factors α_{DC} for the Vogel (1985) frame determined using Design Cases (DC) 1-5 compared against the benchmark GMNIA ultimate load factor α_{GMNIA}. DC1: GNA + τ_g + τ_b + no member imperfections + member check, DC2: GNA + τ_g + H_{ANL} + no member imperfections + member check, DC3: GNIA + τ_g + τ_b + member imperfections (L/1000) + cross-section check, DC4: GNIA + τ_g + τ_b + member imperfections (L/1000) + cross-section check with CSM end points, and DC5: GMNIA + member imperfections (equivalent imperfection) + CSM strain limits.

	GMNIA	DC1	DC2	DC3	DC4	DC5
α_{DC}	1.00	0.85	0.76	0.86	0.91	1.00
$\alpha_{DC}/\alpha_{GMNIA}$	-	0.85	0.76	0.86	0.91	1.00

Table 9. Stiffness reduction factors τ_b calculated for members of the austenitic stainless steel Vogel (1985) frame for Design Cases 1 to 4. DC1: GNA + τ_g + τ_b + no member imperfections + member check, DC2: GNA + τ_g + H_{ANL} + no member imperfections + member check, DC3: GNIA + τ_g + τ_b + member imperfections (L/1000) + cross-section check, and DC4: GNIA + τ_g + τ_b + member imperfections (L/1000) + cross-section check with CSM end points. HNL H_{ANL}

Member	DC1	DC2	DC3	DC4
C11	0.66	-	0.66	0.63
C21	0.30	-	0.30	0.27
C31	0.53	-	0.52	0.49
B11	-	-	-	-
B21	-	-	-	-
C12	0.74	-	0.73	0.71
C22	0.40	-	0.39	0.36
C32	0.64	-	0.63	0.60
B12	-	-	-	-
B22	-	-	-	-
C13	0.82	-	0.81	0.79
C23	0.47	-	0.46	0.43
C33	0.76	-	0.75	0.73
B13	-	-	-	-
B23	-	-	-	-
C14	0.90	-	0.89	0.88
C24	0.63	-	0.63	0.60
C34	0.87	-	0.87	0.85
B14	-	-	-	-
B24	-	-	-	-
C15	0.89	-	0.88	0.87
C25	0.71	-	0.70	0.68
C35	0.87	-	0.86	0.85
B15	-	-	-	-
B25	-	-	-	-
C16	0.98	-	0.98	0.98
C26	0.95	-	0.95	0.94
C36	0.98	-	0.98	0.98
B16	-	-	-	-
B26	-	-	-	-

Table 10. Maximum normalised bending moments within members determined at the ultimate system loads determined for Design Cases 1 to 5 for the Vogel (1985) frame (denoted M_{DC1} to M_{DC5}), with comparative normalised bending moments from GMNIA (denoted M_{GMNIA}). DC1: GNA + τ_g + τ_b + no member imperfections + member check, DC2: GNA + τ_g + H_{ANL} + no member imperfections + member check, DC3: GNIA + τ_g + τ_b + member imperfections (L/1000) + cross-section check, DC4: GNIA + τ_g + τ_b + member imperfections (L/1000) + cross-section check with CSM end points, and DC5: GMNIA + member imperfections (equivalent imperfection) + CSM strain limits.

Members	DC1		DC2		DC3		DC4		DC5	
	M_{DC1}/M_p	M_{DC1}/M_{GMNIA}	M_{DC2}/M_p	M_{DC2}/M_{GMNIA}	M_{DC3}/M_p	M_{DC3}/M_{GMNIA}	M_{DC4}/M_p	M_{DC4}/M_{GMNIA}	M_{DC5}/M_p	M_{DC5}/M_{GMNIA}
C21	0.36	0.96	0.44	1.26	0.38	1.00	0.40	1.05	0.48	1.04
C31	0.55	1.05	0.45	0.99	0.58	1.06	0.63	1.10	0.72	1.03
B11	0.95	1.09	0.83	1.07	0.96	1.08	1.03	1.10	1.05	0.99
C22	0.38	0.96	0.35	1.04	0.40	0.97	0.43	0.98	0.54	1.01
C32	0.56	0.99	0.52	1.04	0.58	0.99	0.62	1.00	0.72	1.00
B12	0.84	1.10	0.75	1.09	0.85	1.09	0.91	1.11	0.88	0.98
C23	0.30	0.89	0.30	1.03	0.32	0.89	0.34	0.88	0.50	1.02
C33	0.54	0.97	0.48	0.99	0.55	0.96	0.59	0.96	0.70	1.00
B13	0.92	1.11	0.83	1.10	0.93	1.10	0.99	1.13	0.94	0.99
C24	0.24	0.89	0.22	0.97	0.25	0.88	0.27	0.86	0.44	1.04
C34	0.58	1.03	0.53	1.03	0.59	1.02	0.62	1.05	0.63	0.98
B14	0.85	1.21	0.76	1.16	0.86	1.20	0.92	1.24	0.79	0.99
C25	0.26	0.92	0.26	1.07	0.26	0.86	0.28	0.83	0.42	0.93
C35	0.69	0.92	0.65	0.99	0.70	0.89	0.74	0.89	0.91	0.98
B15	0.80	1.16	0.72	1.12	0.81	1.15	0.86	1.19	0.77	0.99
C26	0.09	1.23	0.08	1.27	0.09	1.17	0.09	1.16	0.09	0.92
C36	0.79	0.90	0.71	0.94	0.79	0.88	0.84	0.88	1.07	1.00
B16	0.79	1.20	0.71	1.15	0.80	1.20	0.84	1.23	0.73	1.00
Ave.		1.03		1.07		1.02		1.04		0.99
Std.		0.11		0.09		0.11		0.13		0.03
Max.		1.23		1.27		1.20		1.24		1.04
Min.		0.89		0.94		0.86		0.83		0.92

Table 11. Ultimate load factors of the duplex stainless steel multistory asymmetric frame determined using Design Cases 1-5 α_{DC} compared against the benchmark shell FE GMNIA ultimate load factor α_{GMNIA}. DC1: GNA + τ_g + τ_b + no member imperfections + member check, DC2: GNA + τ_g + H_{ANL} + no member imperfections + member check, DC3: GNIA + τ_g + τ_b + member imperfections (L/1000) + cross-section check, DC4: GNIA + τ_g + τ_b + member imperfections (L/1000) + cross-section check with CSM end points, and DC5: GMNIA + member imperfections (equivalent imperfection) + CSM strain limits.

	GMNIA	DC1	DC2	DC3	DC4	DC5
α_{DC}	0.260	0.210	0.208	0.214	0.216	0.260
$\alpha_{DC}/\alpha_{GMNIA}$	1.00	0.81	0.80	0.82	0.83	1.00

Table 12. Stiffness reduction factors calculated for each member in the frame for Worked Example 2.

	τ_b	τ_g
C1	0.977	0.7
C2	0.996	0.7
C3	0.997	0.7
C4	0.996	0.7
B1	-	0.7
B2	-	0.7

Table 13. Required compressive and flexural strengths at the critical cross-section of each member of the frame in Worked Example 2.

	P_r (kN)	M_r (kNm)
C1	1622.0	730.2
C2	1988.7	733.2
C3	831.9	348.3
C4	972.4	348.8
B1	92.1	560.2
B2	91.7	347.9

Table 14. Checks on critical cross-sections of six frame members in Worked Example 2

C1	$\frac{1622.0}{6667.9}+\frac{8}{9}\frac{730.2}{939.2}=0.93$	$0.93\leq 1\therefore$ ok
C2	$\frac{1988.7}{6667.9}+\frac{8}{9}\frac{733.2}{939.2}=0.99$	$0.99\leq 1\therefore$ ok
C3	$\frac{831.9}{2(6667.9)}+\frac{348.3}{939.2}=0.43$	$0.43\leq 1\therefore$ ok
C4	$\frac{972.4}{2(6667.9)}+\frac{348.8}{939.2}=0.44$	$0.44\leq 1\therefore$ ok
B1	$\frac{92.1}{2(6667.9)}+\frac{560.2}{939.2}=0.60$	$0.60\leq 1\therefore$ ok
B2	$\frac{91.7}{2(6667.9)}+\frac{347.9}{939.2}=0.38$	$0.38\leq 1\therefore$ ok